FINAL TECHNICAL REPORT

15031/CCOST/MRP/ 2013: 29/03/2014

"RARE EARTH DOPED CALCIUM ALUMINO SILICATE NANO/MICRO PHOSPHORS: SYNTHESIS, CHARACTERIZATION AND DEVICE PROSPECTS"

Dr. Mrs. Nameeta Brahme

(Professor)

Principal Investigator

School of Studies in Physics & AstroPhysics,

Pt. Ravishankar Shukla University,

Raipur (C.G) - 492010

FINAL TECHNICAL REPORT

CHHATTISGARH COUNCIL OF SCIENCE AND TECHNOLOGY (CCOST)

MIG-25 Indravati Colony, Raipur

1. **Project Report for the Period** : April 2014 – March 2016
2. **Name of the Project** : "Rare Earth Doped $Ca_2Al_2SiO_7$ Nano / Micro Phosphors: Synthesis, Characterization and Device Prospects''. ".
3. **No. & Date of Sanction** : No. 15031/CCOST/MRP/ 2013: 29/03/2014
4. **Name & Address of PI** : Dr. Mrs. Nameeta Brahme (Professor) S.O.S in Physics & Astro Physics, Pt. R.S. University, Raipur (C.G)

5. (A) Amount Sanctioned for Two years (May 2014 – April 2016)

S. No.	Funds	Ist Year(Rs)	IIndYear(Rs)	Total
1.	Staff Salary(PF)@10000/-	1,20,000/-	1,20,000/-	2,40,000/-
2.	Contingency	40,000/-	40,000/-	80,000/-
3.	Minor equipment	1,80,000/-	-	1,80,000/-
	TOTAL	**3,40,000/-**	**1,60,000/-**	**5,00,000/-**

(B) Expenditure:

(i) Ist Year (April 2014 – March 2015): Audited Statement / UC Already Submitted (copy enclosed).

First Year (1st April 2014 – 31st March 2015)				
Funds	Sanctioned (Rs)	Released (Rs)	Expenditure (Rs)	Balance (Rs)
Contingency 1. Chemical Glassware and other items & Advt. of PF 2. Stationary, Books, Reprints 3. TA Expenditure 4. Ordit fees	16,000/- 14,000/- 10,000/- -	16,000/- 14,000/- 10,000/- -	16077/- 14036/- 12,009/- 3200/-	(-)77=00 (-)36=00 (-)2009=00
Equipment: (a) Furnace – 99,750/- (b) CRO – 36081/- (c) Filter – 41,561/-*	1,80,000/-	1,77,392/-	135,831/-	41,561/-
Staff Salary Project Fellow10,000/-(PM)	1,20,000/-	1,20,000/-	1,10,000/- (salary for 11month)	10,000/-
Total	3,40,000/-	3,37,392/-	2,91,153/-	51,561/-

(ii) IInd Year (April 2015 – March 2016): Audited Statement / UC Already Submitted (copy enclosed).

Sr.	Funds	Sanctioned (Rs)	Prev. Balance (Rs)	Released (Rs)	Total (Rs)	Expenditure (Rs)	Balance (Rs)
1.	Staff Salary (PF 10,000 PM)	1,20,000/-	10,000/-	1,20,000/-	1,30,000/-	1,30,000/-	NIL
2.	Contingency						
a.	Chemical Glassware, other & Adv. of PF	16,000/-	--------	16,000/-	16,000/-	16,078/-	(-)78/-
b.	Stationary, books, reprint	14,000/-	----------	14,000/-	14,000/-	14,019/-	(-)19/-
c.	TA Expenditure	10,000/-	---------	10,000/-	10,000/-	11,252/-	(-) 1252/-
3.	Minor Equip.	NIL	41,561/-	NIL	41,561/-	41,561/-	NIL
	Total	1,60,000/-	51,561/-	1,60,000/-	2,11,561/-	2,11,561/-	NIL

6. Name of the Project Fellow (PF) appointed in the project along with dates of joining and leaving.

- **Miss Geetanjali Tiwari: Date of joining: 30/04/2014; Date of leaving: 30/04/2016.**

7. Total work done in the Project (Duration: April 2014 – March 2016)

There are two outstanding processes by which a material can become a generator or origin of light (radiation) after absorbing suitable extraneous primary energy. In one process the absorbed energy is converted (degraded) into low-quantum-energy heat that diffuses through the material which then emits radiation called thermal radiation. In the other process an appreciable part of the absorbed energy is temporarily localized as relatively high-quantum-energy excitation of atoms or small groups of atoms which then emit radiation called luminescence radiation. The term "luminescence" was introduced into literature by Wiedemann in 1888. Luminescence is a general term for the emission of electromagnetic radiation from the substance during or following the absorption of energy from suitable

sources such as UV, γ radiation, X-rays or high energy particle. The energy lifts the atoms of the material into an excited state, and then, because excited states are unstable, the material goes back to its ground state, and the absorbed energy is liberated in the form of either light or heat or both. Luminescence is a consequence of the radiative recombination of the excited electrons/holes. Luminescence process involves at least two steps – **a) Excitation of electronic system of the substance and b) The subsequent emission of photon**. These two steps may or may not be separated by intermediate process. Depending upon types of excitation source there are different types of luminescence – Photoluminescence, Mechanoluminescence, Thermoluminescence, Cathodoluminescence, Electroluminescence, Chemiluminescence, Lyoluminescence, Sonoluminescence etc.

Mechanoluminescence (ML) is an important physical phenomenon where an emission of light is observed due to mechanical deformation of materials when they are subjected to some mechanical stress like rubbing, cleavage, compressing, impulsive crushing, grinding, shaking etc. [1-5]. Emission via ML has also been observed due to many other processes e.g. thermal shocking (immediate cooling or heating), phase transition and separation of two different materials in contact. ML can be due to both the elastic and plastic deformation of the solids. Depending upon the nature of mechanical stress, ML has also been termed as fractoluminescence, elasticoluminescence, plasticoluminescence and triboluminescence in the literature [6, 7]. Many organic and inorganic crystals, polymers, ceramic and glasses have shown to exhibit ML [8]. ML has found various important applications such as impact sensors in spacecrafts (the emission intensity can be used to determine the kinetic energy of impact), fracture sensor, damage sensor, sensor for stress and its distribution in the solids, crack propagation in solids and understanding of the basic mechanism of crack growth [9-11]. Chandra et al. have presented various theoretical studies on various kind of ML [4, 12-15]. Thermoluminescence (TL) in solids is the light emission (mainly visible) that takes place during heating of a solid following an earlier absorption of energy from radiation. The essential condition for TL to occur in an insulator or semiconductor is that the material must have been previously exposed to radiation. Once the TL emission has been observed, the material will not show it again after simply cooling the specimen and reheating it, but has been re exposed to radiation to obtain TL again. TL, although based upon the same fundamental principles as other luminescence processes, is conventionally is misnomer since the heat radiation is only a stimulant and not an exciting agent. Urbach (1930) is usually credited with suggesting TL as a potentially useful research tool for trap-level analysis. A

large number of dielectric materials exhibit TL emission , including minerals, rocks, inorganic semiconductors and insulators, glasses and ceramics, organic compounds, biological materials and biochemicals. Materials such as LiF, $CaSO_4$, CaF_2, BeO, Al_2O_3 and $Li_2B_4O_7$ are most extensively studied TL materials because of their applications in dosimetry.

The rare earth - activated silicates are an important class of phosphorescence materials because of their high quantum efficiency in visible region [16], long persistence of phosphorescence, good stability, color purity and good chemical, thermal and radiation resistance [17-21]. The potential benefit of rare earth ions as an activator has now well established in the field of luminescence. Different activators contribute significantly in tailoring the afterglow properties of phosphors from few seconds to many hours. In Eu the life time of 5d-4f transitions are about 3 orders of magnitude shorter than 4f-4f transition lifetime exhibited by other lanthanides and thus are of immense importance.

This research project proposed to discover some new mechanoluminescent and thermoluminescent phosphor and then to characterize the phosphor and finally optimized luminescent aluminate phosphors according to different parameters. These optimized phosphors will be suitable for development of pressure sensors and can also be used for dosimetry purposes. The phosphors were synthesized using Combustion Technique, which is novel, economic and takes less time to prepare. The total work carried out in the project has been on the lines proposed in the original research proposal. The overall progress of the work in the total project duration has been quite satisfying, as envisaged. The outcomes of the present investigations have been published in the form of papers in various National/International Journals. The total work done in the present project is briefly described in the next section and the list of research papers is given below along with the copy of paper attached here with.

Broad Objectives:

1. Synthesis of rare
2. Characterization
3. Photoluminescen
   phosphor after γ-

1. Synthesis of rare ea

The raw materials are c
(99.99%)], silicon di-
dysprosium nitrate [Dy(
grade (A.R.), were em
Stoichiometric compositi
the total oxidizing and r
and urea were mixed to
resulting paste is transfer
maintained at 600°C. I
decomposition with the
ammonia). The process b
The solution underwent s
and voluminous ash. The
out of the furnace and th
The powders were gro
,$Ca_2Al_2SiO_7:Eu^{3+}$ and Ca

The following phosp
$Ca_2Al_2SiO_7:Ce^{3+}$,Ca
annealed at 1100°C

Summary of Total Work-done

Broad Objectives:

1. Synthesis of rare earth doped $Ca_2Al_2SiO_7$ phosphors by combustion assisted method.
2. Characterization of Phosphors.
3. Photoluminescence, Mechanoluminescence & Thermoluminescence study of the phosphor after γ- irradiation.

1. Synthesis of rare earth doped $Ca_2Al_2SiO_7$ phosphors by combustion-assisted method:

The raw materials are calcium nitrate [$Ca(NO_3)_2$ (99.99%)], aluminum nitrate [$Al(NO_3)_3.9H_2O$ (99.99%)], silicon di-oxide [SiO_2 (99.99%)], cerium nitrate [$Ce(NO_3)_3.6H_2O$(99.99%)], dysprosium nitrate [$Dy(NO_3)_3.6H_2O$] and europium nitrate [$Eu(NO_3)3.6H_2O$] all of analytical grade (A.R.), were employed in this experiment. Urea [NH_2CONH_2] were added as fuel. Stoichiometric composition of the metal nitrates (oxidizers) and urea (fuel) were calculated using the total oxidizing and reducing valences of the components. Weighed quantities of each nitrate and urea were mixed together and crushed into mortar for 2 hour to form a thick paste. The resulting paste is transferred to crucible and introduced into a vertical cylindrical muffle furnace maintained at 600°C. Initially the mixture boils and undergoes dehydration followed by decomposition with the evolution of large amount of gases (oxides of carbon, nitrogen and ammonia). The process being highly exothermic continues and the spontaneous ignition occurs. The solution underwent smoldering combustion with enormous swelling, producing white foamy and voluminous ash. The flame persists for approximate 30 seconds. The crucible is then taken out of the furnace and the foamy product can easily be milled to obtain the precursor powder. The powders were ground and annealed at 1100°C for 4hour to obtain $Ca_2Al_2SiO_7:Ce^{3+}$,$Ca_2Al_2SiO_7:Eu^{3+}$ and $Ca_2Al_2SiO_7:Dy^{3+}$ phosphors.

The following phosphors were prepared –
$Ca_2Al_2SiO_7:Ce^{3+}$,$Ca_2Al_2SiO_7$: Eu^{3+} and $Ca_2Al_2SiO_7:Dy^{3+}$ at initiating temp. 600 °C and annealed at 1100°C for 4 hour with different dopant concentration.

2. Characterization of Phosphors:

The phosphors were characterized by different techniques viz. / XRD / TEM/ SEM / EDX.

2.1 XRD Spectra of $Ca_2Al_2SiO_7$: Ce^{3+}

The crystal structure and crystallite size was calculated by powder X-ray diffraction analysis. XRD results indicate that in the phosphors prepared at 600˚C, a peak located at 2θ =31.4˚, belonging to the characteristic peak of $Ca_2Al_2SiO_7$: Ce^{3+}, is weak and peak coexisted at 27˚ attributed to SiO_2 is high. It is clear that at 600˚C, some the SiO_2 remains unreacted and characteristic peak of SiO_2 is observed. When sample annealed at 1100˚C for 3hour, SiO_2 reacted completely and pure phase of $Ca_2Al_2SiO_7$ found. Fig.1 shows the XRD pattern of $Ca_2Al_2SiO_7$:Ce^{3+}phosphors annealed at 1100˚C for 4 hours. By annealing the sample at 1100˚C the extra peak of SiO_2 is removed and it results in enhancement of the intensity of the diffraction peak and reduction in the full – width at half maximum, due to the improvement of crystalline and grain growth. The XRD analysis revealed that the appropriate introduction of an activator (Ce^{3+}) did not influence the crystal structure of the phosphor matrix, including that Ca^{2+} ions can be partly replaced by Ce^{3+} ions without any change of crystal structure. Fig.2 indicates that the crystal structure of $Ca_2Al_2SiO_7$ is mainly tetragonal and matches well to the JCPDS data file no. 35-0755. The diffraction intensity is maximum for (2 1 1) plane having 2θ= 31.4˚. This structure, a member of the melilite group, is crystallized based on the tetragonal lattice system with space group P-421m (No. 113) with cell parameters a = b= 0.7690 nm and c = 0.5063 nm. The average crystallite size was calculated from the XRD pattern using Debye Scherrer relation $D = k\lambda / \beta\cos\theta$, where D is the crystallite size for the (hkl) plane, k is dimensionless shape factor, with a value close to unity, λ is the wavelength of the incident X- ray radiation Cu Kα (0.154 nm), β is the full

width at half maximum (FWHM) in radian, and θ is the corresponding angle of Bragg diffraction. In the case of (211) plane, average crystallite size of $Ca_2Al_2SiO_7:Dy^{3+}$ phosphor was ~ 50.85nm.

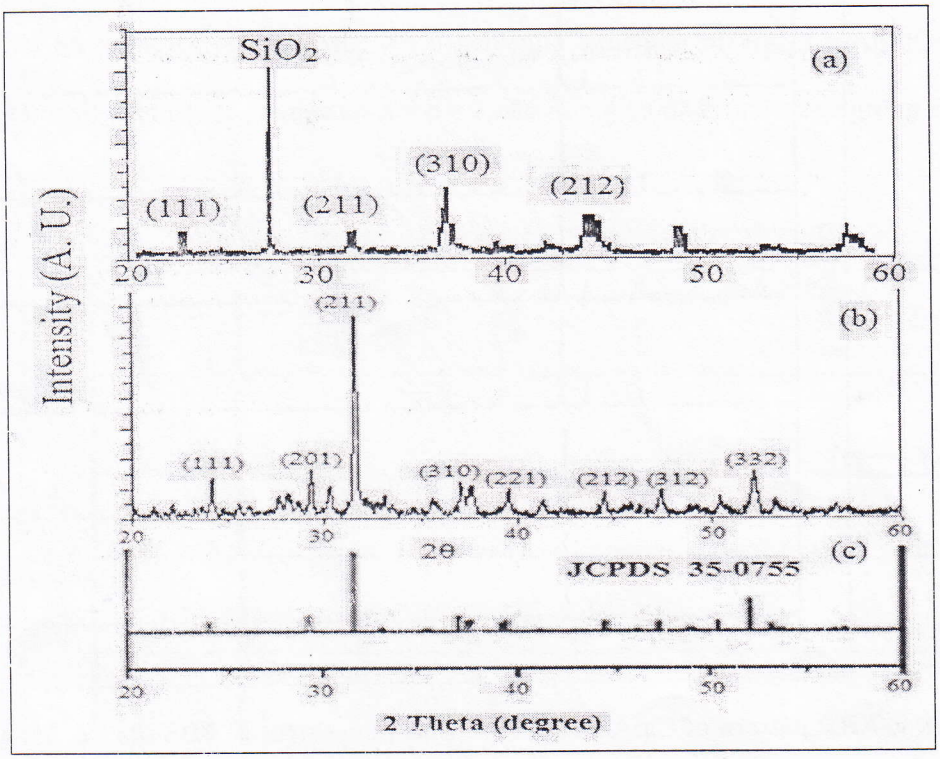

Fig.1 X-ray diffraction pattern of $Ca_2Al_2SiO_7$: Ce^{3+}(2mol %) phosphor
(a) Prepared at 600°C
(b) Annealed at 1100°C (c) JCPDS data file no. 35-0755

2.2 XRD Spectra of $Ca_2Al_2SiO_7$: Dy^{3+}

The phase structure of the prepared $Ca_2Al_2SiO_7$: Dy^{3+} phosphor was analyzed by the XRD (Fig.2).The position of diffraction peaks of the prepared $Ca_2Al_2SiO_7$: Dy^{3+} phosphor is well matched with the standard JCPDS data of the compound $Ca_2Al_2SiO_7$ having pure tetragonal phase (JCPDS file No.35-0755). The small amount of doped rare earth ions (Dy^{3+}) has virtually

no effect on the phase structure of pure $Ca_2Al_2SiO_7$ phosphor. No other crystalline phases were detected. The diffraction intensity is maximum for (2 1 1) plane having 2θ= 31.4°.

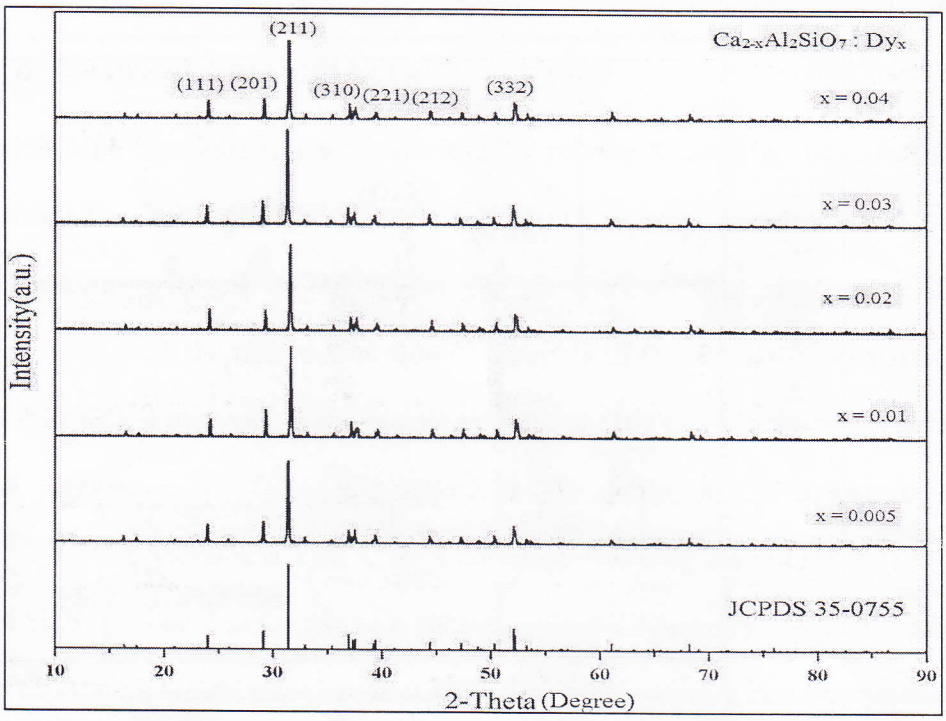

Fig.2 XRD pattern of $Ca_2Al_2SiO_7$: Dy^{3+} phosphors with JCPDS file No. 35 –0755

This structure, a member of the melilite group, is having space group P-421m (No. 113) with cell parameters a = b= 0.7690 nm and c = 0.5063 nm. The average crystallite size was calculated from the XRD pattern using Debye Scherrer relation $D = k\lambda / \beta\cos\theta$, where D is the crystallite size for the (hkl) plane, k is dimensionless shape factor, with a value close to unity, λ is the wavelength of the incident X- ray radiation Cu Kα (0.154 nm), β is the full width at half maximum (FWHM) in radiation, and θ is the corresponding angle of Bragg diffraction. In the case of (211) plane, average crystallite size of $Ca_2Al_2SiO_7$:Dy^{3+} phosphor was ~ 50.15nm.

2.3 XRD Spectra of $Ca_2Al_2SiO_7$: Eu^{3+}

The XRD patterns of $Ca_2Al_2SiO_7$:Eu^{3+} phases with different doping contents are shown in Fig.3 and all profiles were found to be in good agreement with JCPDS-card (No. 35-0755), which indicates that no impurity phase exists. As a gehlenite structure mineral, $Ca_2Al_2SiO_7$ has a tetragonal unit cell with lattice parameters a = b = 7.686 Å, c = 5.068 Å and space group P 4 21m (No. 113).

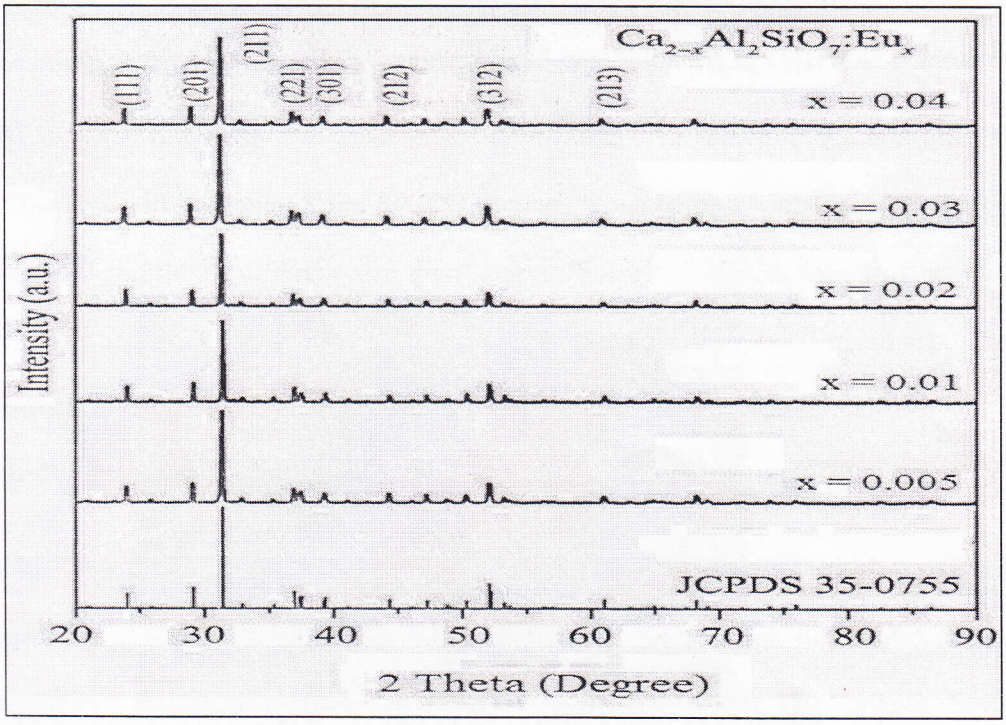

Fig. 3 XRD patterns of $Ca_2Al_2SiO_7$: Eu^{3+} phosphors

In the structure of $Ca_2Al_2SiO_7$, the cations are localized at three types of sites an eightfold coordinated site called Thomson cube (TC) occupied by Ca^{2+}, a regular tetrahedral site (T_1) fully occupied by Al^{3+} ions, and a very distorted tetrahedral site (T_2), where Si^{4+} ions and Al^{3+} ions are statistically distributed. Therefore, based on the effective ionic radii r of cations with different coordination number (CN) reported by Shannon, we propose that Eu^{3+} ions are expected to and,

in fact, occupy the Ca^{2+} sites preferably, because the ionic radius of Eu^{3+} (r = 1.066 Å when CN = 8), are close to that of Ca^{2+} (r = 1.12 Å when CN = 8). Since both four- coordinated Al^{3+} (r = 0.39 Å) and Si^{4+} (r = 0.26 Å) sites are relatively small for Eu^{3+} to occupy, we there by conclude that Eu^{3+} tends to prefer the Ca^{2+} sites due to size consideration. The average crystallite size was calculated from the XRD pattern using Debye Scherrer relation $D = k\lambda / \beta\cos\theta$, where D is the crystallite size for the (hkl) plane, k is dimensionless shape factor, with a value close to unity, λ is the wavelength of the incident X- ray radiation Cu Kα (0.154 nm), β is the full width at half maximum (FWHM) in radiation, and θ is the corresponding angle of Bragg diffraction. In the case of (211) plane, average crystallite size of $Ca_2Al_2SiO_7:Eu^{3+}$ phosphor was ~ 50.9nm.

2.4 Transmission electron microscopy (TEM) $Ca_2Al_2SiO_7:Ce^{3+}$

Fig. 4 TEM image of the $Ca_2Al_2SiO_7:Ce^{3+}$ (2mol %) phosphor

Fig.4 shows the transmission electron microscope image of $Ca_2Al_2SiO_7:Ce^{3+}$ phosphor. TEM image shows that the shape of the particle is tetragonal structure and the particle size ranges in between 10 nm and 50nm. So we conclude that, transmission electron microscopy results are in good agreement with the result of the XRD studies.

2.5 Transmission electron microscopy (TEM) $Ca_2Al_2SiO_7:Dy^{3+}$

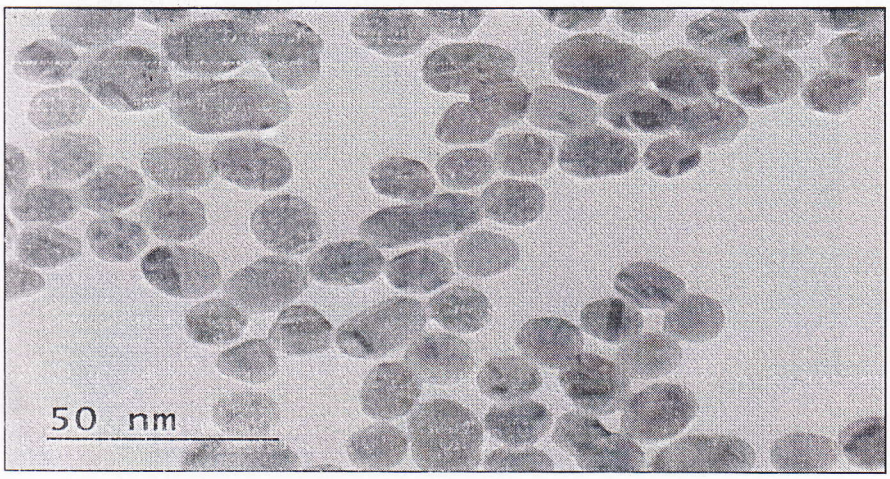

Fig. 5. TEM image of $Ca_2Al_2SiO_7$: Dy^{3+} (1mole%) phosphor

The grain size of $Ca_2Al_2SiO_7$:Dy^{3+}phosphor is shown in Fig.5. The TEM images confirm the grain size of the prepared phosphor. From the TEM image, it can be observed that the prepared sample consists of grain with different size distribution. Moreover, agglomeration of powder particles was also observed, which is due to the high-temperature heat treatment. The transmission electron microscopy results are in good correlation with the XRD result.

2.6 Transmission electron microscopy (TEM) $Ca_2Al_2SiO_7$:Eu^{3+}

Fig.6 shows the transmission electron microscopy images of $Ca_2Al_2SiO_7$:Eu^{3+} which consist of aggregated particles with size smaller than 50 nm. Variation in particle size might also due to agglomeration of very fine particles due to high temperature heat treatment. TEM images shows that the shape of the particle is tetragonal structure and particle size ranges in between 20 and 50 nm. So we conclude that, transmission electron microscopy results are in good agreement with the result of the XRD studies.

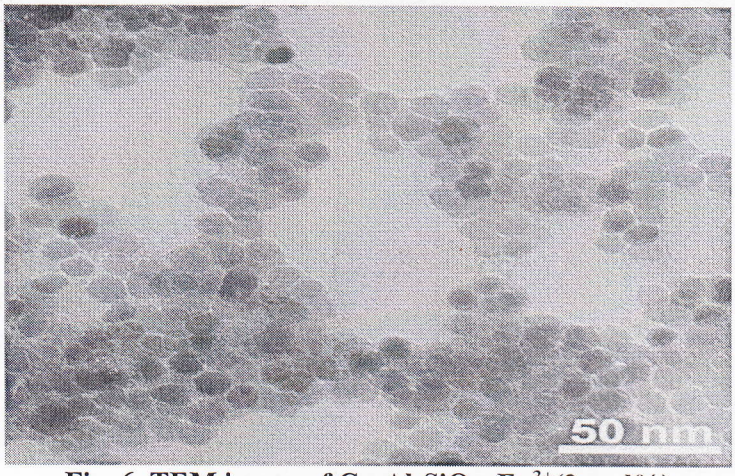

Fig. 6. TEM image of $Ca_2Al_2SiO_7$:Eu^{3+}(2 mol%)

2.7. Scanning electron microscopy (SEM)

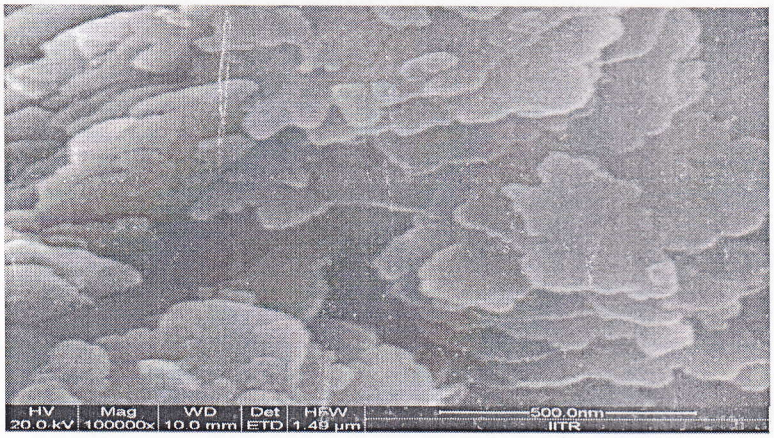

Fig. 7 SEM image of the $Ca_2Al_2SiO_7$:Ce^{3+} (2mol %) phosphor

The SEM micrograph of the $Ca_2Al_2SiO_7$: Ce^{3+} powder annealed at 1100°C for 3h is shown in the Fig. 7. Morphological study reveals that the prepared phosphor is having flake type structure and has large extent of agglomeration. The agglomeration is also present due to high temperature heat treatment.

2.8 Scanning electron microscopy (SEM)

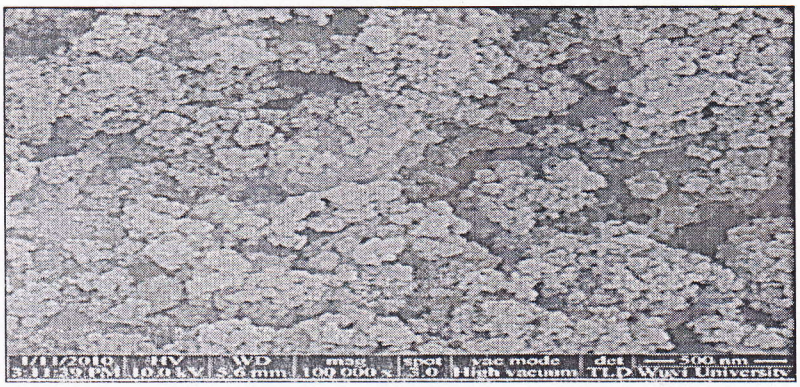

Fig.8. SEM image of $Ca_2Al_2SiO_7$:Dy^{3+}(1mol%) phosphor

Fig.8 shows the SEM micrograph of the $Ca_2Al_2SiO_7$:Dy^{3+}phosphor. The microstructure of the sample reflects the inherent nature of the combustion process. When a gas is escaping under high pressure during combustion process, pores are formed with the formation of small particles near the pores. The non-uniform and irregular shapes of the particles as shown can be attributed to the non-uniform distribution of temperature and mass flow in the combustion flame. The particle was almost spheroidal and has some extent of agglomeration.

2.9. Scanning electron microscopy (SEM)

Fig.9 shows the SEM micrograph of the $Ca_2Al_2SiO_7$:Eu^{3+}. The microstructure of the sample reflects the inherent nature of the combustion process. When a gas is escaping under high pressure during combustion process, pores are formed with the formation of small particles near the pores. The non-uniform and irregular shapes of the particles as shown can be attributed to the non-uniform distribution of temperature and mass flow in the combustion flame. The particle was almost spheroidal and has some extent of agglomeration.

3h is
e type
o high

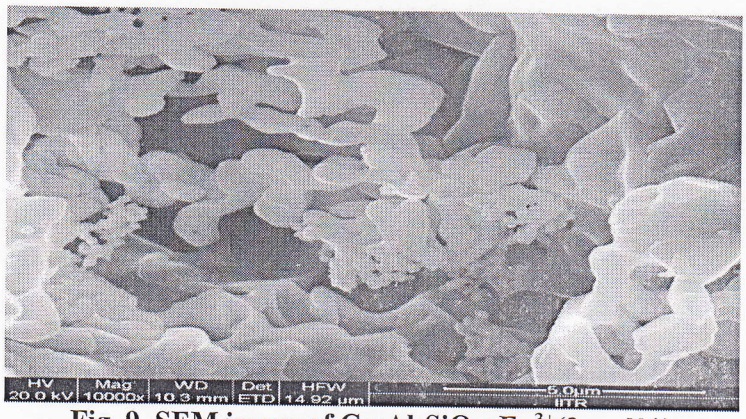

Fig. 9. SEM image of $Ca_2Al_2SiO_7$:Eu^{3+}(2 mol%)

2.10. Energy dispersive X-ray spectroscopy (EDX)

Fig.10 shows the Energy dispersive X-ray spectroscopy (EDX) spectra of the prepared sample. EDX is a standard procedure for identifying and quantifying elemental composition of sample area as small as a few nanometers. The existence of Cerium (Ce) in the prepared phosphor could be clearly seen from the corresponding EDX spectra. Their appeared no other emissions apart from calcium (Ca), aluminum (Al), silicon (Si), oxygen (O) and cerium (Ce) in the $Ca_2Al_2SiO_7$: Ce^{3+} EDX spectra of the phosphor.

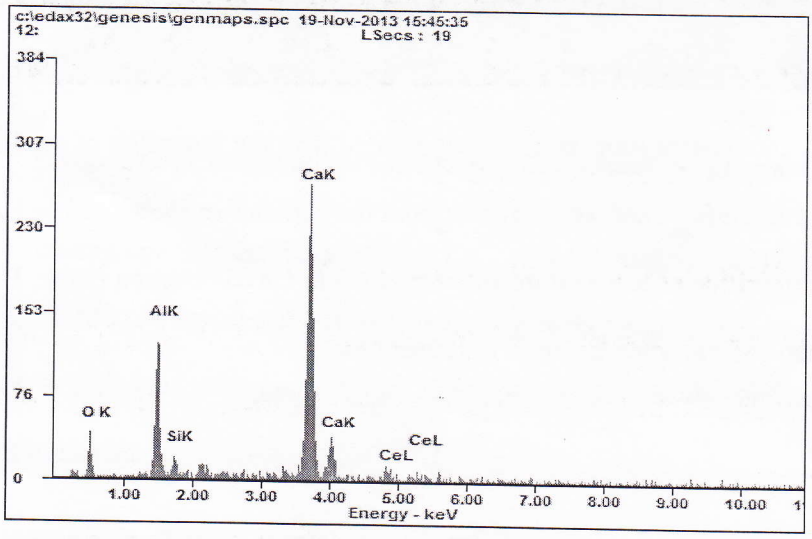

Fig. 10. EDX of Ce Doped (2mol %) $Ca_2Al_2SiO_7$ phosphor

2.11. Energy dispersive X-ray spectroscopy (EDX)

Fig.11 shows the Energy dispersive X-ray spectroscopy (EDX) spectra of the prepared sample. EDX is a standard procedure for identifying elemental composition of sample area as small as a few nanometers. The existence of Dysprosium (Dy) in the prepared phosphor could be clearly seen from the corresponding EDX spectra. No other emissions has appeared apart from calcium (Ca), aluminium (Al), silicon (Si), oxygen (O) and Dysprosium (Dy) in the $Ca_2Al_2SiO_7$: Dy^{3+} EDX spectra of the phosphor.

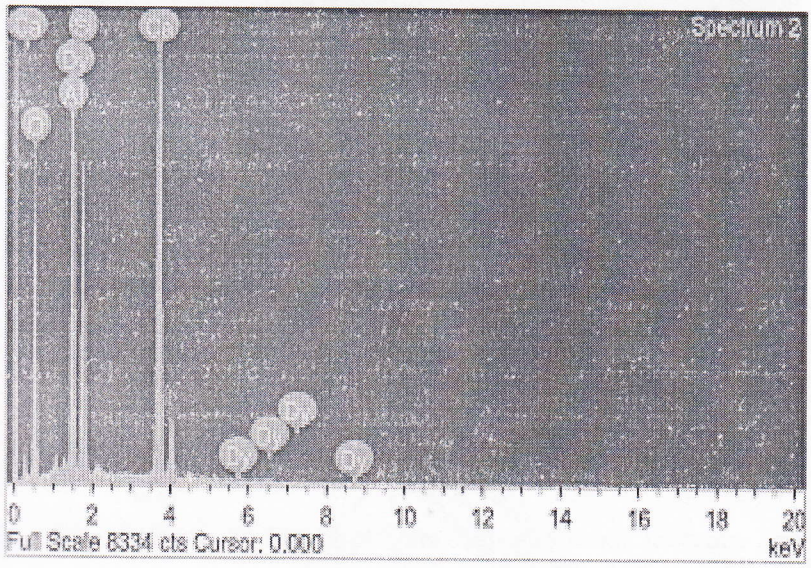

Fig. 11. EDX spectra of $Ca_2Al_2SiO_7$:Dy^{3+}(1mole%) phosphor

2.12. Energy dispersive X-ray spectroscopy (EDX)

Fig.12 shows the Energy dispersive X-ray spectroscopy (EDX) images of $Ca_2Al_2SiO_7$:Eu^{3+}. The chemical composition of the powder sample has been measured using EDX spectra. EDX is a standard procedure for identifying and quantifying elemental composition of sample area as a few nanometers. The existence of europium (Eu) is clear in their corresponding EDX spectra.

Their appeared no other emission apart from calcium (Ca), aluminium (Al), silicon (Si) and oxygen (O) in $Ca_2Al_2SiO_7$: Eu^{3+} EDX spectra of the phosphor. In EDX spectra, the presence of Ca, Al, Si, O and Eu, intense peak are present which preliminary indicates the formation of $Ca_2Al_2SiO_7$: Eu^{3+}phosphor.

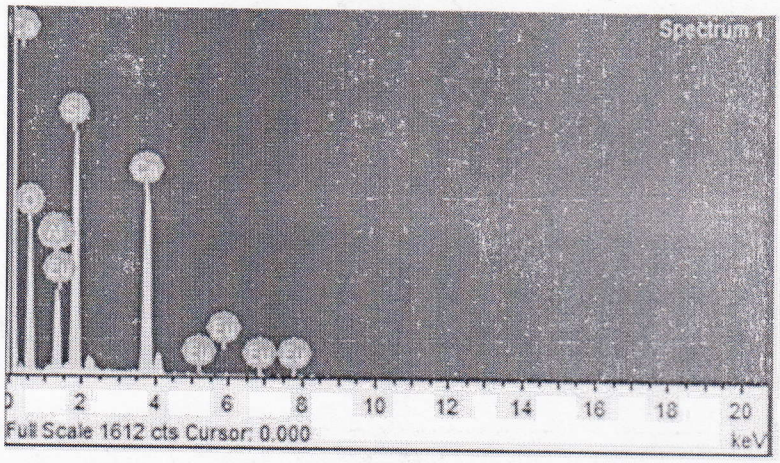

Fig. 12. EDX image of $Ca_2Al_2SiO_7$:Eu^{3+}(2 mol%)

3. Photoluminescence, Mechanoluminescence & Thermoluminescence study of the phosphor after γ- irradiation.

3.1. Photoluminescence (PL) $Ca_2Al_2SiO_7$:Ce^{3+}

The excitation and emission spectra are presented in Fig.13, $Ca_2Al_2SiO_7$: Ce^{3+} exhibits a broad emission band centered on 400nm. This band results from the $5d^1$ to $4f^1$ transition configuration of Ce^{3+} ions. The spectrum is unsymmetrical, consisting of several bands. The excitation spectra indicate that at least two absorption bands can be observed for $Ca_2Al_2SiO_7$: Ce^{3+}. They are located at about 330nm and 310nm. $Ca_2Al_2SiO_7$: Ce^{3+} emits strong UV– violet emission.

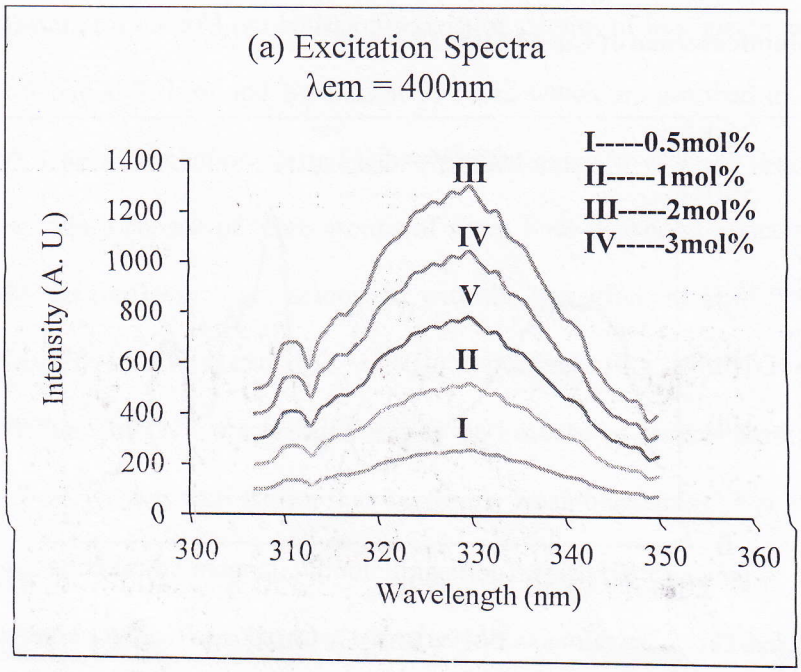

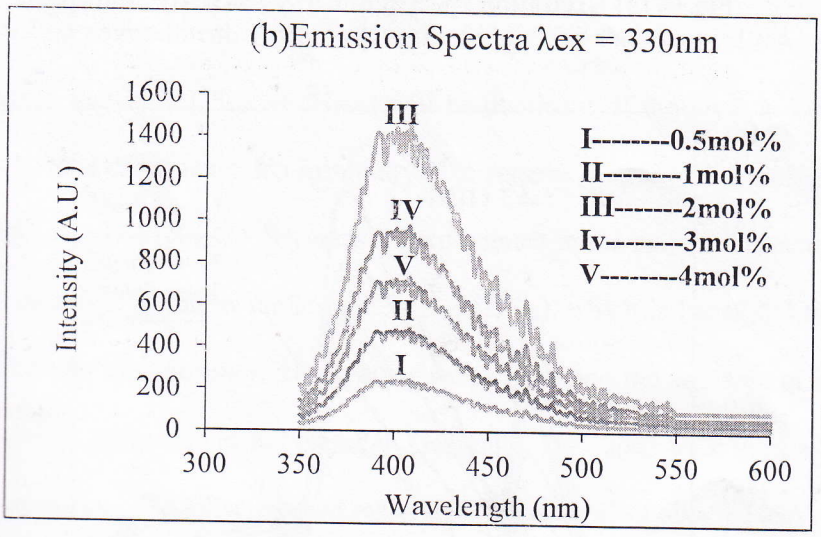

Fig.13 (a) Excitation spectra of $Ca_2Al_2SiO_7:Ce^{3+}$(2mole %)phosphor

(b) Emission spectra of $Ca_2Al_2SiO_7:Ce^{3+}$phosphor

3.2. Photoluminescence of $Ca_2Al_2SiO_7:Dy^{3+}$

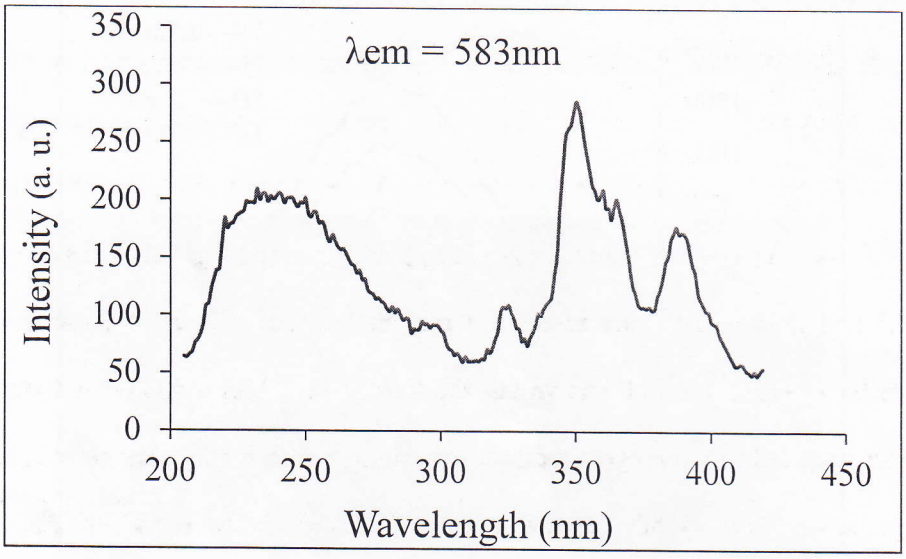

Fig.14 (a) Excitation spectra of $Ca_2Al_2SiO_7:Dy^{3+}$phosphor

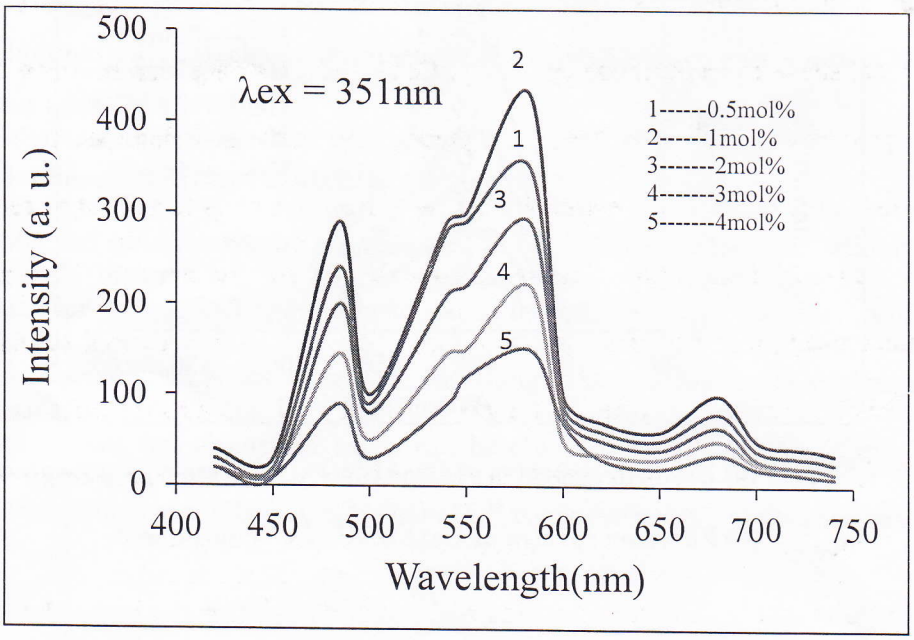

Fig.14 (b) Emission spectra of $Ca_2Al_2SiO_7:Dy^{3+}$phosphor

The excitation spectra for the 583 nm emission consist of a series of line spectra in 300–400 nm with the strongest one at 351nm and weakest at 391 nm, which are ascribed to the transitions from the ground state to excitation states in the $4f^9$ configuration of Dy^{3+} [Fig. 14(b)] . The emission spectra mainly consist of three groups of sharp lines peaked at about 484(blue), 583 (yellow) and 680 nm (red),which are associated with the transitions of Dy^{3+} from the excited state $^4F_{9/2} \rightarrow {}^6H_{15/2}$, $^4F_{9/2} \rightarrow {}^6H_{13/2}$ and $^4F_{9/2} \rightarrow {}^6H_{11/2}$ respectively [Fig. 14(a)]. One can also find that the emission lines of Dy^{3+} are broadened may be because of several Stark levels for the excited state $^4F_{9/2} \rightarrow {}^6H_J$. It is well known that the former weak blue emission at 484nm ($^4F_{9/2} \rightarrow {}^6H_{15/2}$) is corresponded to the magnetic dipole transition, which hardly changes with the crystal field strength around Dy^{3+}. While the later stronger yellow emission at 583 nm ($^4F_{9/2} \rightarrow {}^6H_{13/2}$) belongs to the hypersensitive forced electric dipole transition, which is strongly influenced by the outside surrounding environment. According to the Judd–Ofelt theory, a yellow emission due to the electric dipole transition ($^4F_{9/2} \rightarrow {}^6H_{13/2}$) will be dominant, if the Dy^{3+} is located at a low symmetry local site without inversion symmetry. Conversely, a strong blue emission due to the magnetic dipole transition ($^4F_{9/2} \rightarrow {}^6H_{15/2}$) will predominate in the emission spectra. In our case, the dominated emission is yellow emission ($^4F_{9/2} \rightarrow {}^6H_{13/2}$), which is beneficial to decrease the colour temperature of the phosphor. The synthesis technique and the structure of matrix greatly influence the optical properties of the material. Generally, Dy^{3+} ions were used as codopants in the developed aluminate and silicate based materials. When divalent alkaline earth ions, such as Ca^{2+} or Sr^{2+}, is substituted by trivalent Dy^{3+} in the alkaline earth silicates and aluminates, various defects are induced due to the charge compensation mechanism. In the Eu^{2+} and the Dy^{3+} co-doped materials, most of the excitation energy will be transferred from the host or from the Dy^{3+}

to the Eu^{2+}; hence only 5d-4f emissions of Eu^{2+} can be observed. However, in Dy^{3+} singly doped samples, Dy^{3+} is not only an activator itself but also generates traps.

3.3. Photoluminescence of $Ca_2Al_2SiO_7$:Eu^{3+}

The photoluminescence properties of $Ca_2Al_2SiO_7$: Eu^{3+} host were investigated by the excitation and emission spectra at room temperature. The excitation spectra of $Ca_2Al_2SiO_7$: Eu^{3+} (2 mol%) in the range of 200 – 600 nm monitored at 619 nm emission is shown in Fig. 15(a). The broad band extending from 240–340 nm is associated with charge transfer (CT) transition from 2p orbital of O^{2-} ions to the 4f orbital of Eu^{3+} ions, while the sharp lines correspond to direct excitation of f – f shell transitions of Eu^{3+} ions $^7F_0 \rightarrow {}^5F_2$ (279 nm), $^7F_0 \rightarrow {}^5H_6$ (319 nm), $^7F_0 \rightarrow {}^5H_3$ (328 nm), $^7F_0 \rightarrow {}^5D_4$ (363 nm), $^5G_4$ (383 nm), $^5L_6$ (394 nm), $^5D_3$ (419 nm), $^5D_2$ (466 nm), $^5D_1$ (534 nm) and $^5D_0$ (589 nm), respectively. The prepared $Ca_2Al_2SiO_7$: Eu^{3+} phosphor can be excited by near UV (NUV) at about 394 nm effectively. So, it can match well with UV and NUV-LED, showing a great potential for practical applications (Q. Zhang J. Wang, M. Zhang, W. Ding, Q. Su 2007). As seen in Fig. 15(a), the intensity of the transition at 394 nm is the highest in the spectra. Fig. 15 (b) shows the emission spectrum of $Ca_2Al_2SiO_7$ Eu^{3+} (0.5, 1, 2, 3, 4mol %) in the wavelength range of 500 - 750 nm under 394 nm excitation. There are five main sharp emission peaks at near 580, 589, 619, 658 and 703 nm, among which the intensity of 619 nm line is the highest. It is concluded that the emissions are caused by the f – f forbidden transitions of Eu^{3+} with $4f^6$ electron configuration, corresponding to $^5D_0 \rightarrow {}^7F_0$ (579 nm), $^7F_1$ (589 nm, 602 nm), $^7F_2$ (615nm, 619 nm) and $^7F_3$ (651 nm, 658 nm), $^7F_4$ (693nm, 703 nm), respectively. The orange emission at about 589 nm belongs to the magnetic dipole $^5D_0 \rightarrow {}^7F_1$ transition of Eu^{3+}, and the transition hardly varies with the crystal field strength. The red emission at 619 nm ascribes to the electric dipole $^5D_0 \rightarrow {}^7F_2$ transition of Eu^{3+}, which is very

sensitive to the local environment around the Eu^{3+}, and depends on the symmetry of the crystal field. It is found that the 589 and 619 nm emissions are the two strongest peaks, indicating that there are two Ca^{2+} sites in the $Ca_2Al_2SiO_7$ lattice. One site, Ca (I), is inversion symmetry and the other site, Ca (II), is non inversion symmetry. When doped in $Ca_2Al_2SiO_7$ the Eu^{3+} ions occupied the two different sites of Ca (I) and Ca (II). For the phosphor $Ca_2Al_2SiO_7$: Eu^{3+} prepared in our experiment, the strongest orange emission peak is located at 589 nm will be dominated. It can be presumed that Eu^{3+} ions mainly occupy with an inversion symmetric center in host lattice.

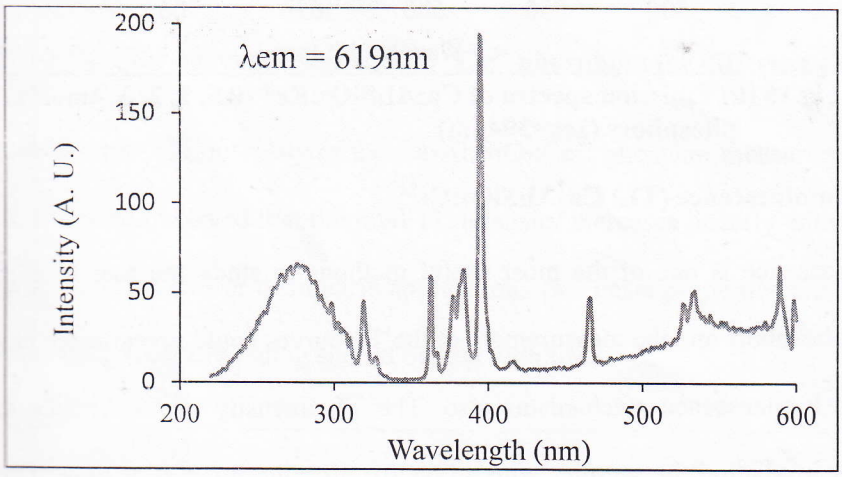

Fig. 15 (a) Excitation spectra of $Ca_2Al_2SiO_7$:Eu^{3+}(2mol%) phosphor (λ_{em} = 619nm)

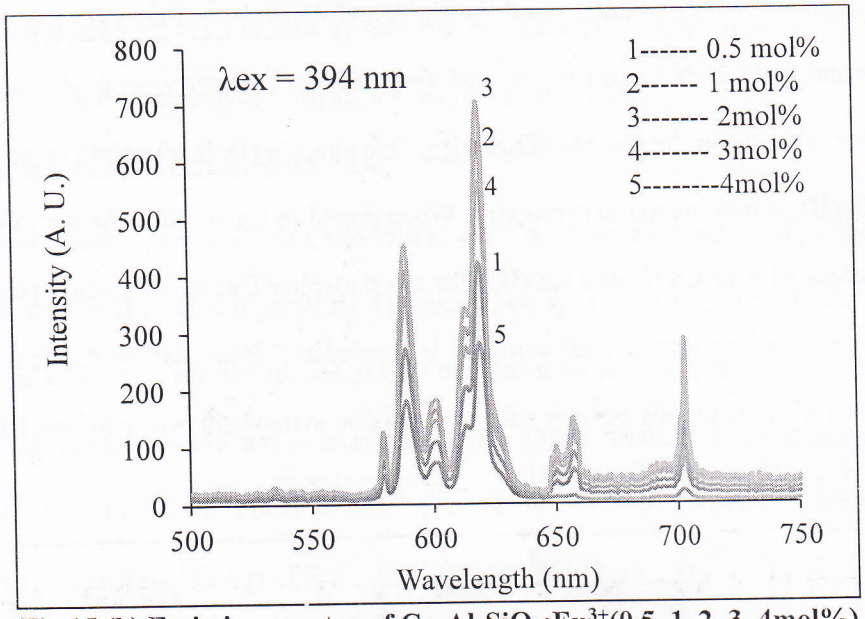

Fig.15 (b) Emission spectra of $Ca_2Al_2SiO_7:Eu^{3+}$(0.5, 1, 2, 3, 4mol%) phosphors (λex=394nm)

3.4. Thermoluminescence (TL) $Ca_2Al_2SiO_7:Ce^{3+}$

Thermoluminescence is one of the most useful methods to study the trap level for persistent luminescent phosphors and the measurement of the TL curves could reveal some new facts about the persistent luminescence mechanisms also. The TL intensity of $Ca_2Al_2SiO_7$ samples were recorded after irradiating the samples with γ rays for different interval of time. The variation in TL intensity with irradiation time is shown in Fig. 16(a). A broad peak at 125^{0}C suggests existence for trapping level. It was found that the TL intensity increases with increasing γ exposure time and it becomes maximum for 1180Gy irradiation time. It is well known that a higher trap density normally leads to a higher after glow intensity and longer persistence, and the intensity of the TL peaks is proportional to the trap density. Usually when a trivalent ion sits in a divalent ion site some defects will be created, producing defect related traps that then result in a long after glow.

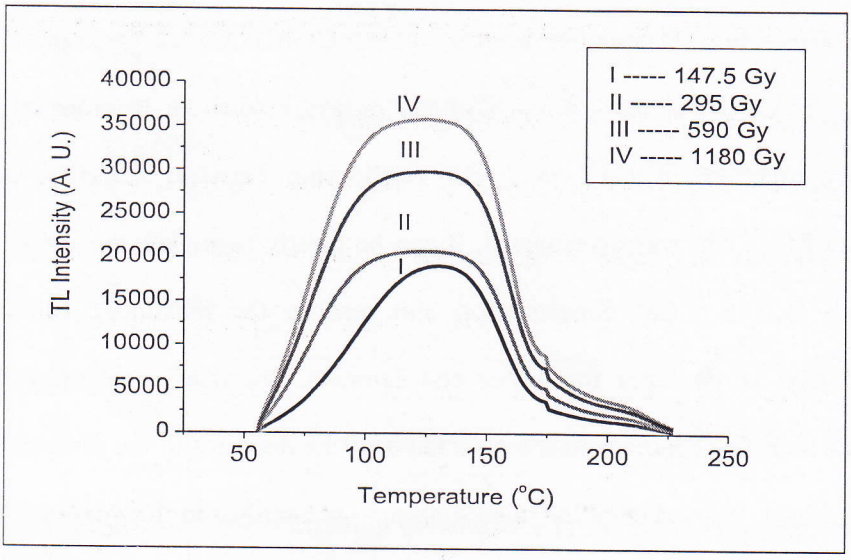

Fig.16 (a) TL glow curves of $Ca_2Al_2SiO_7$: Ce^{3+} phosphors for different γ dose

Fig. 16(b) shows the total TL intensity of the $Ca_2Al_2SiO_7$:Ce^{3+} phosphor measured at different γ exposure time. It can be observed that the total TL intensity increases linearly with increase in γ exposure time up to 1180Gy. For dosimetric applications two basic properties are, firstly, linear behavior with the dose secondly fading should be less with time.

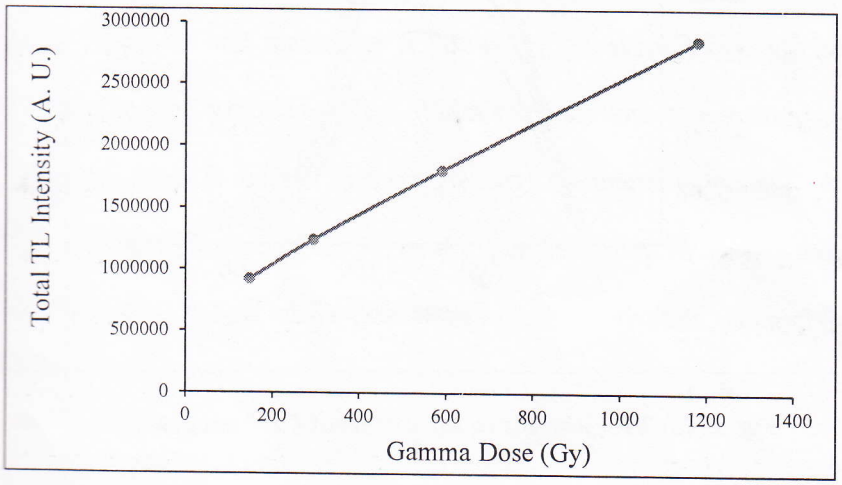

Fig. 16(b) Graph between Total TL intensity of $Ca_2Al_2SiO_7$: Ce^{3+} phosphors and gamma irradiation dose

Fig.17 shows the TL emission intensity of the $Ca_2Al_2SiO_7$: Ce^{3+} samples with various concentrations of Ce^{3+} (x = 0.5 - 4 mol.%) under γ rays irradiation. In order to optimize the luminescence properties of Ce^{3+} ions, the relationship between emission intensity and concentration of Ce^{3+} ion was investigated. It can be clearly seen that the emission intensity increases with increasing Ce^{3+} concentration and reaches the maximum value for 2 mol.% of Ce^{3+} and then it descends for higher concentration. Increase in emission intensity with increase in the activator concentration was because of the decrease in the distance between the activator ions. Later, the concentration quenching may be ascribed to the migration of excitation energy to the quenching centers (traps) or to the cross relaxation (exchange interaction) between neighboring Ce^{3+} ions.

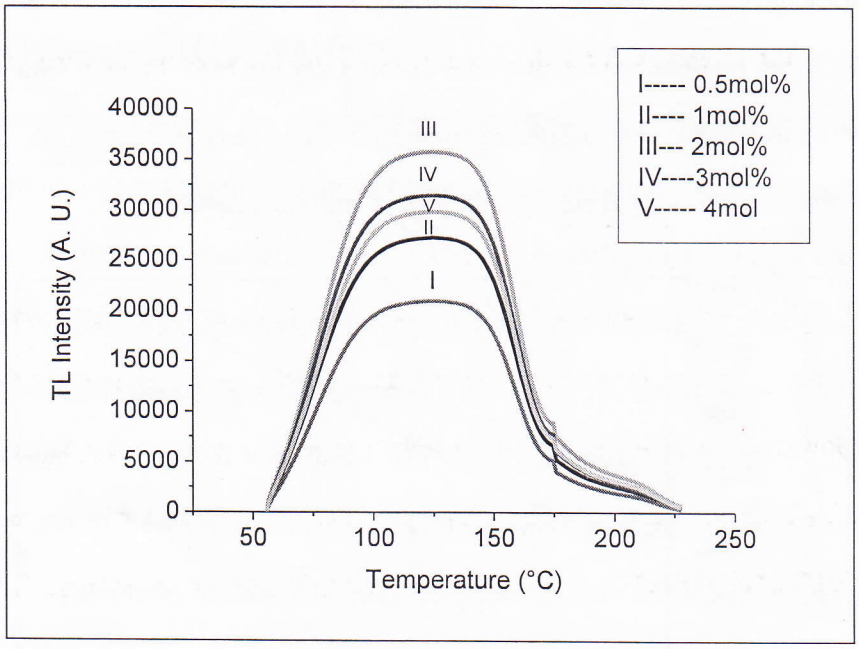

Fig. 17(a) TL glow curve for different Ce^{3+} concentration

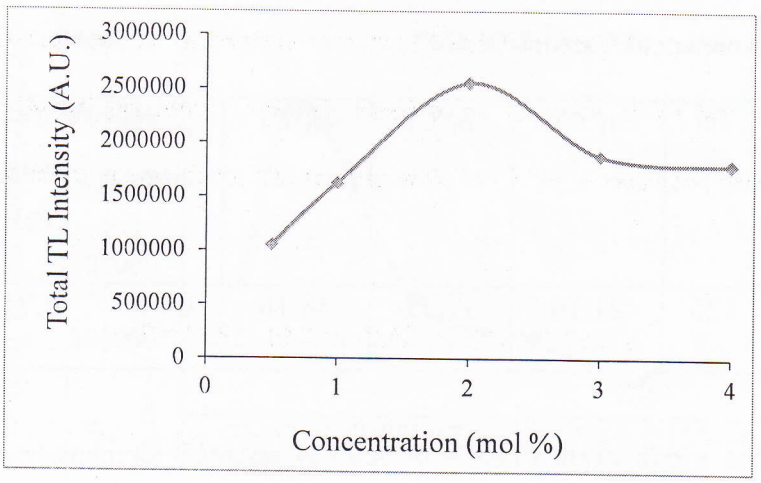

Fig. 17(b) Ce^{3+} concentration dependence of the total TL peak intensity

The TL parameters i.e. activation energy (E) and frequency factor (s) for the prominent glow peaks of prepared phosphor were calculated using the peak shape method are shown in Table 1. The activation energy E for the sample with 1180 Gy γ- radiation time was calculated by the formula

$$E = [2.52+10.2(\mu_g - 0.42)](k_B T_m^2/\omega) - 2k_B T_m$$

Where ω, the full Width at half maximum is known as the shape parameter and defined as $\omega=\delta+\tau$, with δ being the high temperature half-Width and τ the low- temperature half width. The asymmetric glow-peak shape is defined by the asymmetry parameter $\mu_g = \delta/\omega$, k_B is Boltzmann's constant, and T_m is the temperature of the TL peaks. The frequency factor was calculated by the formula $S=\beta E/kT^2_m * \exp(E/kT_m)$, where β=heating rate, E= activation energy, T_m= maximum temperature.

Table 1. TL parameters of $Ca_2Al_2SiO_7:Ce^{3+}$

γ dose (Gy)	Heating Rate	Tm (°C)	τ(°C)	δ(°C)	ω(°C)	$\mu_g = \delta/\omega$	Activation energy E(eV)	Frequency factor (S^{-1})
1180	5	125	21.14	17.12	38.16	0.45	0.71	$2.21*10^{14}$

It is reported that a trap depth (0.65 – 0.75eV) is essential for phosphors to show long persistence, so the trap depth, 0.69eV of $Ca_2Al_2SiO_7$: Ce^{3+} phosphors is suitable for a long afterglow.

3.5. Thermoluminescence of $Ca_2Al_2SiO_7$: Dy^{3+}

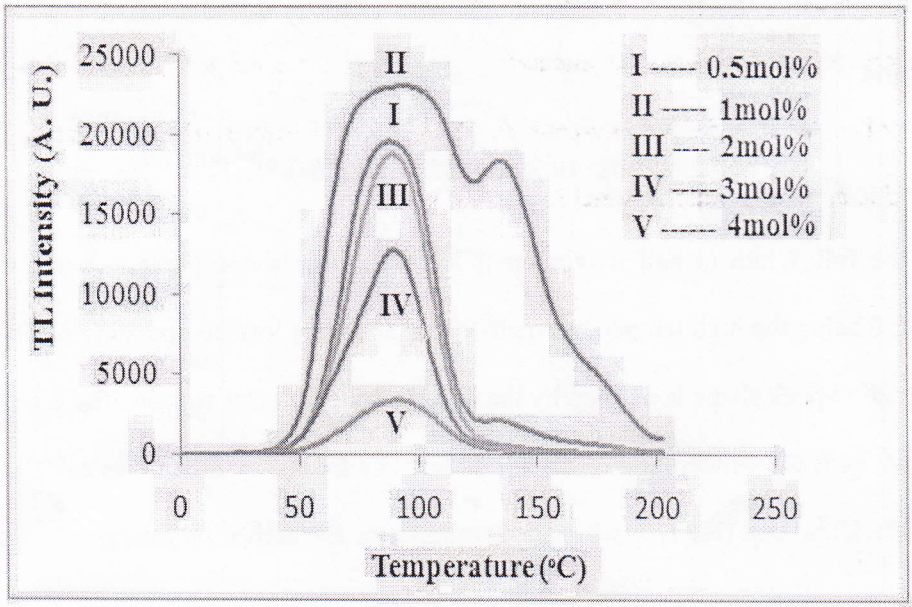

Fig.18 (a) TL glow curve for different Dy^{3+} concentration

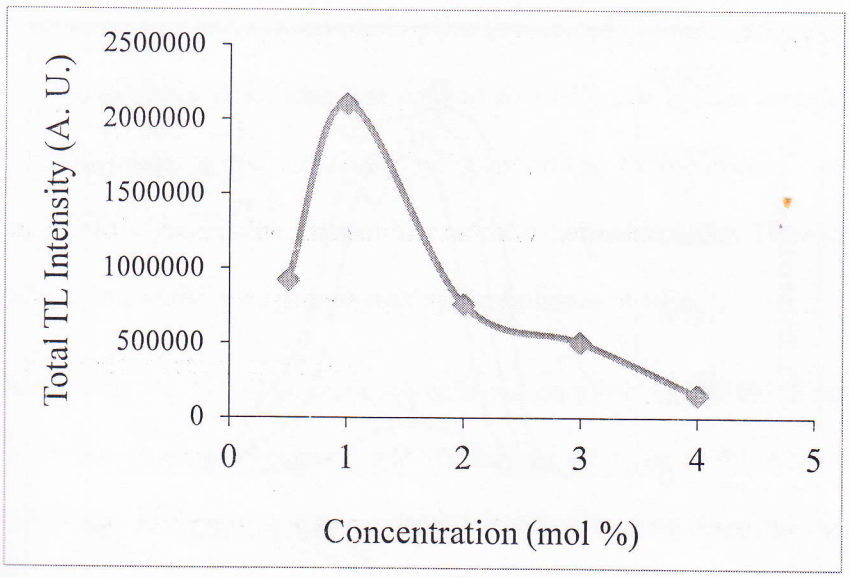

Fig.18 (b) Dependendy of total TL intensity on Dy^{3+} concentration

Fig.18 shows TL glow curves of $Ca_2Al_2SiO_7:Dy^{3+}$phosphors. As the concentration of Dy^{3+} ions increased from 0.5 to 4 mol%, the intensities gradually increased and reached the maximum value at 1mol%. With a further increase of Dy^{3+} ion concentration, the intensity decreased remarkably due to concentration quenching.

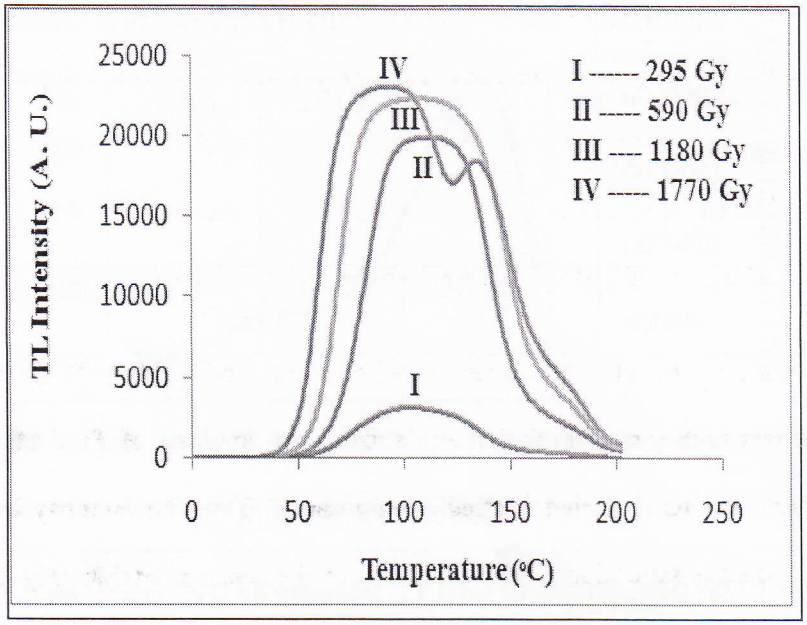

Fig.19 (a) TL glow curves for different γ dose

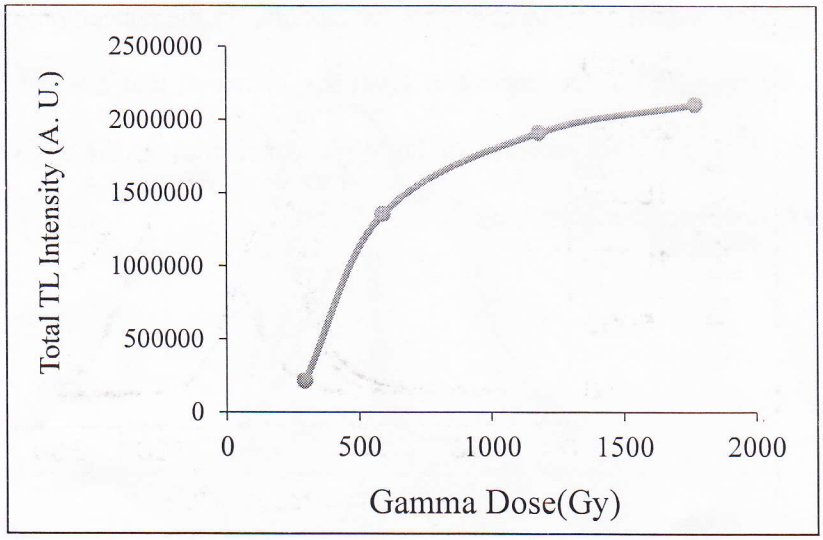

Fig.19 (b) Dependence of Peak TL intensity on γ–dose

Fig. 19 shows the dependence of TL intensity on γ-dose of $Ca_2Al_2SiO_7:Dy^{3+}$(1 mol%) sample. Observation has taken for different gamma radiation doses: 295, 590, 1180, 1770Gy.It is found that Total TL intensity is initially increasing with γ- dose and it seems to be saturated at 1180 Gy.

Under exposure to γ-ray, electron hole pairs are created. Some of the released electrons are captured by the impurity RE^{3+} ions that convert to RE^{2+}. The hole is captured in the host related centers. Warming of the irradiated samples causes these holes to get un-trapped successively at different temperatures, depending on their thermal stability. The excited impurity ions by decaying to its ground state give characteristic emission of RE^{3+}.

The increase in the TL / ML intensity with γ-dose attributed to the increase of active luminescent centers with γ-ray irradiation and subsequent emission of TL / ML is due to re-oxidation of RE^{2+} into RE^{3+} during heating / deformation. Thus the intensity increases in the initial stage. The dosage saturation can be explained on the assumption that only limited number of RE ions are available for charge reduction with γ-ray irradiation.

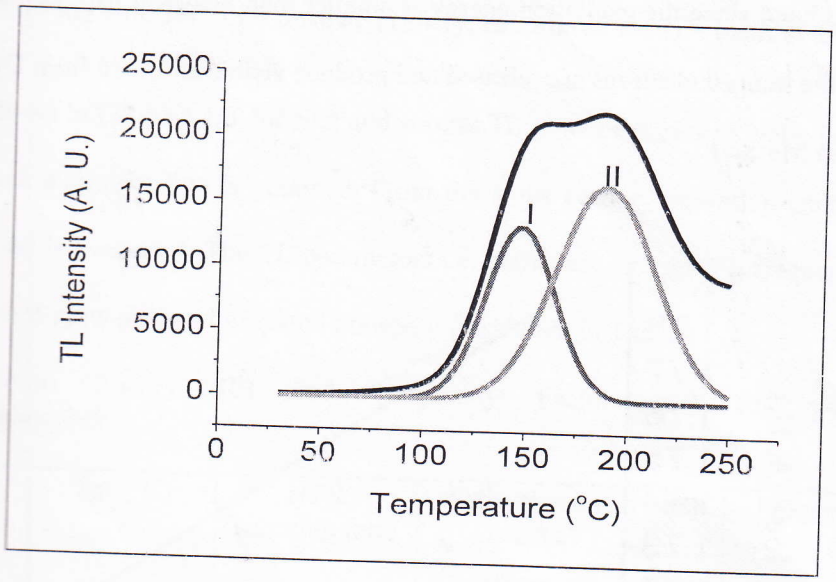

Fig. 20 TL glow curve of $Ca_2Al_2SiO_7$: $Dy^{3+}$for 1180Gy and peak deconvolution

The peak deconvolution of TL curve is shown in Fig. 20. It has two dominant bands peaked at 147°C and 189°C. Dy^{3+} is an important rare-earth ion in the development of phosphors with

long-lasting afterglow, playing a crucial role. The dopant $Dy^{3+}$is a famous trap-creating ion, which can greatly prolong the afterglow. It is reasonable to consider that the role of doping Dy^{3+}ions is to introduce new types of traps or significantly increase the concentration of traps responsible for the afterglow. We tentatively propose two possible types of the traps in $Ca_2Al_2SiO_7:Dy^{3+}$. In the first case, Dy ions act as not only luminescence centers but also traps, since Dy ions can form some electron trap levels in the band gap. In the other case, the traps can occur because of the charge compensation due to the substitution of divalent $Ca^{2+}$and Al^{2+}ions in the $Ca_2Al_2SiO_7:Dy^{3+}$host by trivalent Dy^{3+}ions. The fact that the characteristic excitation of Dy^{3+}can lead to the afterglow emission from Dy^{3+}suggests that the trap filling process may occur through the direct transfer of electrons from the excited states of Dy^{3+} to trap centers and not via conduction band since the excitation energy is smaller than the band gap. During the afterglow emission, the trapped electrons are released and produce visible emission from Dy^{3+}.

Initial Rise Method

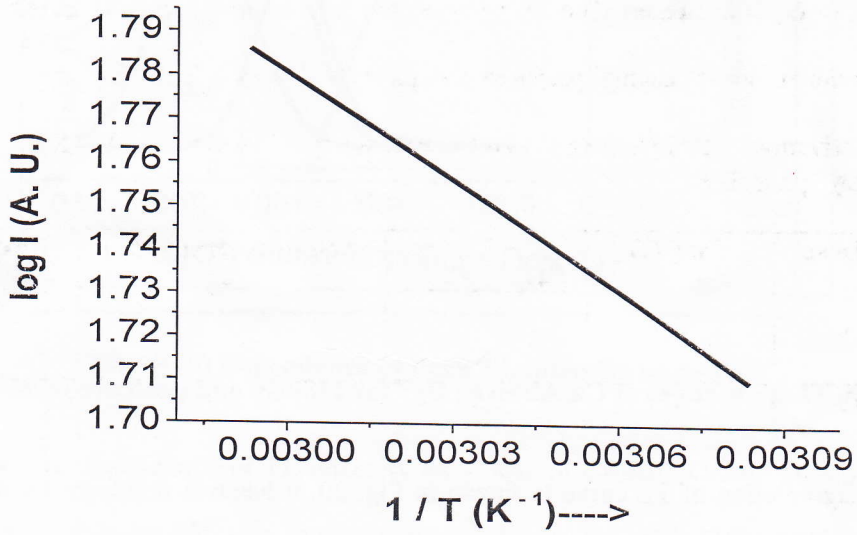

Fig. 21 Plot of log I vs. 1/T for γ dose of 1180 Gy, calculated for I^st peak at 147⁰C

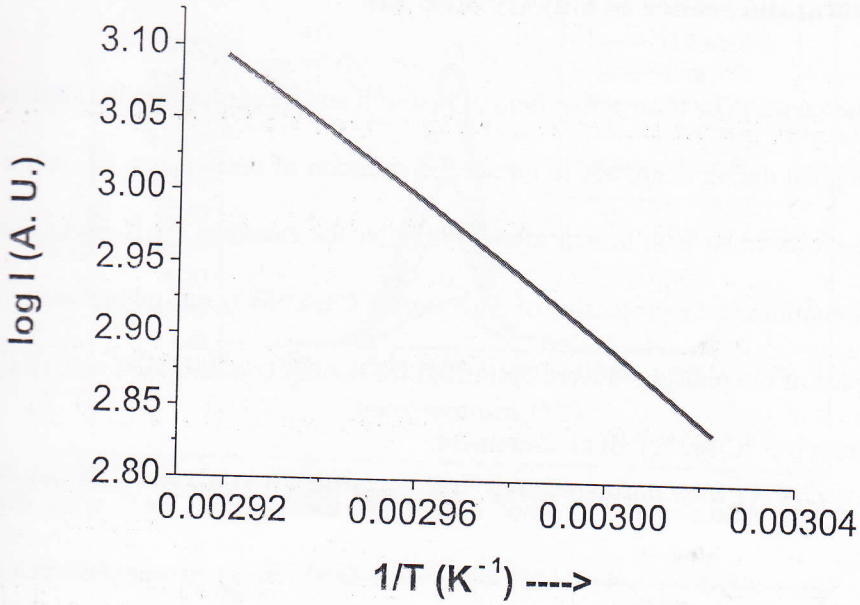

Fig. 22 Plot of log I vs. 1/T for γ dose of 1180Gy, calculated for IInd peak at 189^{0}C

Fig. 21 and 22 shows ln (TL) Vs 1/T for first and second TL glow peak respectively. In applying initial rise method, a straight line is obtained. From the slope of line, activation energy E and frequency factor (s) is evaluated. The TL parameters i.e. activation energy (E), frequency factor (s) for the prominent glow peaks of prepared phosphor are shown in Table 2

Table2. Activation Energy (E) and Frequency Factor (s^{-1}) for γ-irradiated $Ca_2Al_2SiO_7:Dy^{3+}$phosphor.

Peak	γ – Dose	Tm (°C)	HTR (Heating rate)	Activation energy (E) (eV)	Frequency factor (S^{-1})
IInd	1180Gy	147	10	0.78	$1.12*10^{14}$
IInd	1180Gy	189	10	1.29	$2.01*10^{14}$

3.6. Thermoluminescence of $Ca_2Al_2SiO_7$: Eu^{3+}

Thermoluminescence (TL) is an active field of research and its application in radiation dosimetry and archaeological dating continues to attract the attention of researchers. TL is the light that a solid sample emits when it is heated after irradiation for example, by X-rays, γ-rays and UV light. Thermoluminescence properties of Eu^{3+} doped $Ca_2Al_2SiO_7$ phosphors were investigated. TL glow curves of the phosphors were optimized for doping concentration and γ exposure time. The heating rate is 5 °C/sec for all measurement.

Fig. 23(a) shows the TL glow curves of $Ca_2Al_2SiO_7$: Eu^{3+} with different Eu^{3+} concentrations (x = 0.5, 1, 2, 3, 4 mol %) with γ dose for 1770 Gy. It was observed that total TL intensity increased with increasing doping concentrations of Eu^{3+} and attained maximum for 2 mol% concentrations. Further increment in doping concentration decreased the total TL intensity of the phosphor. An increase in the activator concentrations increased the energy stored by the ions, consequently TL intensity increased. It is well known that the luminescence intensity of the phosphor is strongly influenced by the activator concentration. As the distance between the activators got shorter, the interaction of the ions increased and the probability of the energy transfer between same ion increased, consequently luminescence intensity decreased. There is an optimum in the activator concentration, as seen in Fig. 23(a) and (b).

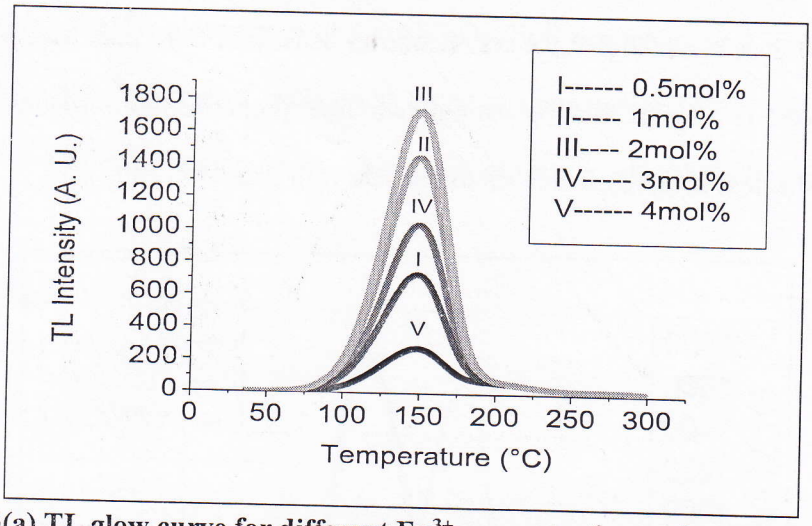

Fig. 23(a) TL glow curve for different Eu^{3+} concentration with 1770Gy γ dose

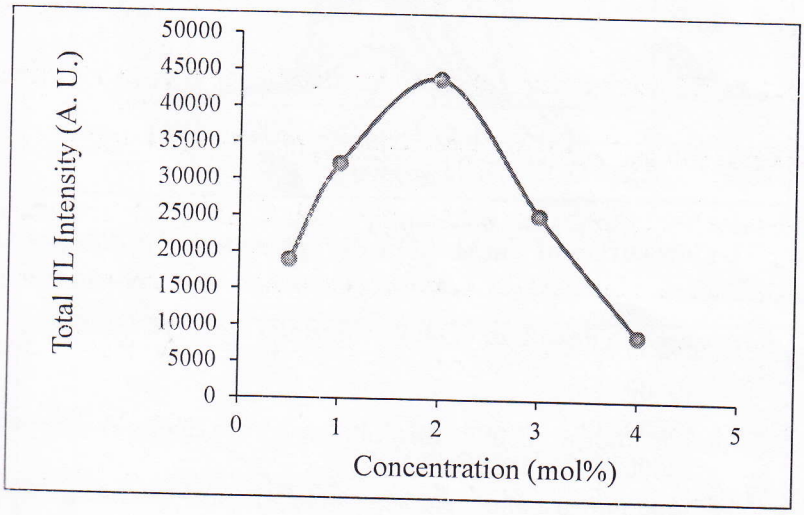

Fig. 23 (b) Eu^{3+} concentration dependence of the total TL peak intensity

The TL measurement was carried out between room temperature and 300 °C. Fig. 24(a) shows the TL glow curve of $Ca_2Al_2SiO_7$: Eu^{3+} phosphors for different γ exposure time, from 295Gy to 1770Gy. Fig. 24(b) shows the total TL intensity of the $Ca_2Al_2SiO_7$:Ce^{3+} phosphor measured at different γ exposure time. It can be observed that the total TL intensity increases linearly with increase in γ exposure time up to 1770Gy. The TL intensity was maximum for 1770 Gy γ-

irradiation time. It is assumed that the charge carrier density of traps may have increased with increasing γ dose. For dosimetric applications two basic properties are essential, firstly, linear behavior with the dose secondly fading should be less with time.

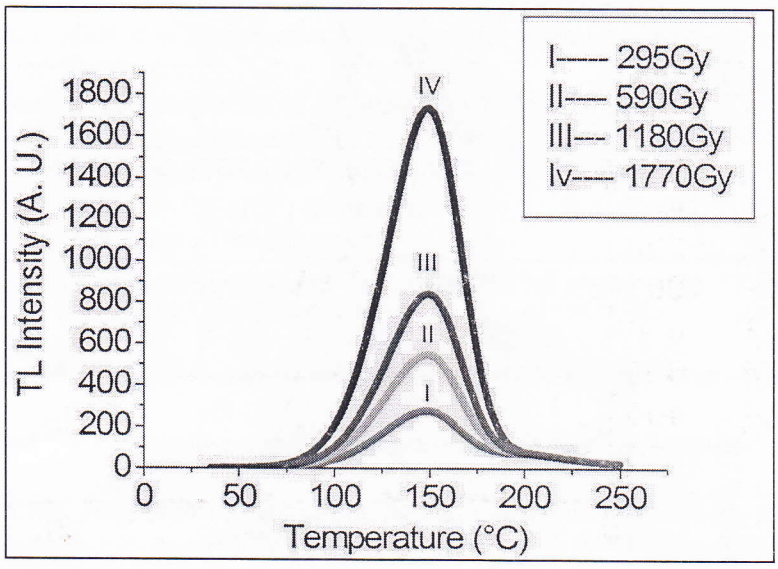

Fig.24 (a) TL glow curves of $Ca_2Al_2SiO_7$: Eu^{3+} phosphors for different γ dose

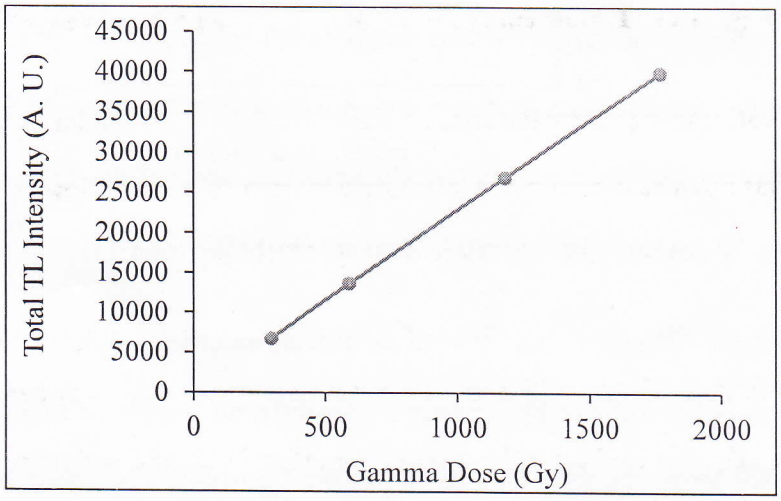

Fig.24 (b) Graph between total TL intensity of $Ca_2Al_2SiO_7$: Eu^{3+} Phosphors and gamma irradiation dose

Fig. 24 (c) shows the TL glow curve of $Ca_2Al_2SiO_7$: Eu^{3+} phosphor for 1770Gy γ rays. The obtained peak is deconvoluted in two peaks, found at temperature 142°C and 152°C. These peaks are due to different trapping levels. The reason of traps in phosphors is usually the lattice defects.

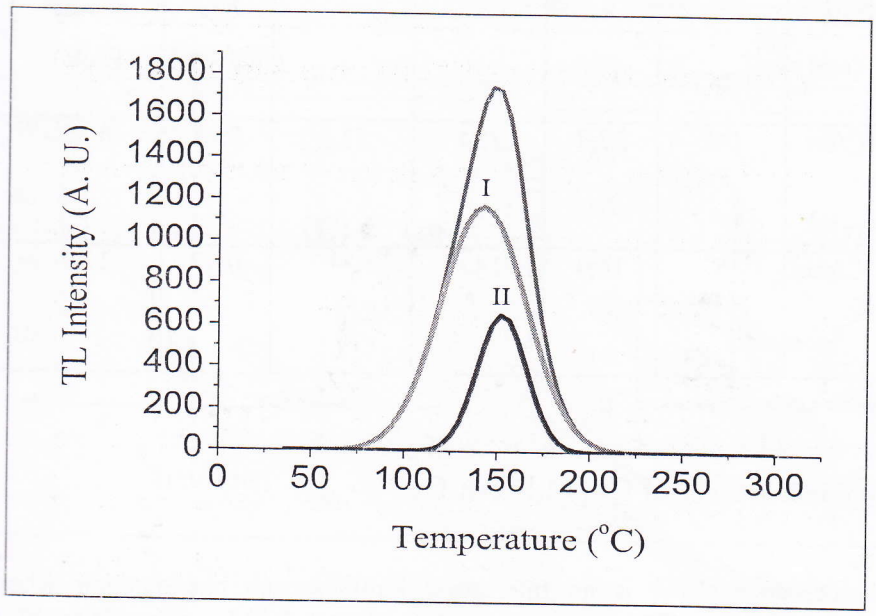

Fig. 24(c) TL glow curve for 1770Gy and peak deconvolution

The thermal activation energy E for the sample with 1770 Gy γ- radiation time (associated with the trap depth) was calculated from the glow peak parameters using the following equation.

$$E = [\, 2.52 + 10.2\,(\mu - 0.42)\,]\,(\, kT_m^2 / \omega\,) - 2kT_m$$

Where $\omega = \tau + \delta$ is the total half width intensity, τ is the half width at the low temperature side of the peak ($\tau = T_m - T_1$), δ is the half width towards the fall-off side of the glow peak ($\delta = T_2 - T_m$), and T_m is the peak temperature at the maximum. The $\mu = \delta/\Omega$, is shape factor to differentiate between first and second order TL glow peak. The frequency factor was calculated by the formula $S = \beta E / kT^2_m * \exp(E/kT_m)$, where β=heating rate, E= activation energy, T_m= maximum

temperature. The TL parameters i.e. activation energy (E) and frequency factor (s) for the prominent glow peaks of prepared phosphor are shown in Table 3.

Table 3. TL parameters of $Ca_2Al_2SiO_7:Eu^{3+}$

γ dose (Gy)	Heating Rate	Tm (°C)	τ(°C)	δ(°C)	ω(°C)	$\mu_g = \delta/\omega$	Activation energy E(eV)	Frequency factor (S^{-1})
1770(I^{st} Peak)	5°C/sec	142	27.7	25.8	53.5	0.48	0.85	$2.83*10^{11}$
1770(IInd Peak)	5°C/sec	152	16.4	14.6	31	0.47	1.34	$1.87*10^{14}$

3.7. Mechanoluminescence of $Ca_2Al_2SiO_7$: Ce^{3+}

Mechanoluminescence (ML) is an interesting luminescence phenomenon where by light emission in solids is caused by cutting, grinding, cleaving, shaking, rubbing, scratching, and compressing or by crushing of solids. ML also appears during the deformation caused by the phase transition or growth of certain crystals. In these ML studies, an impulsive deformation technique has been used for measurements.

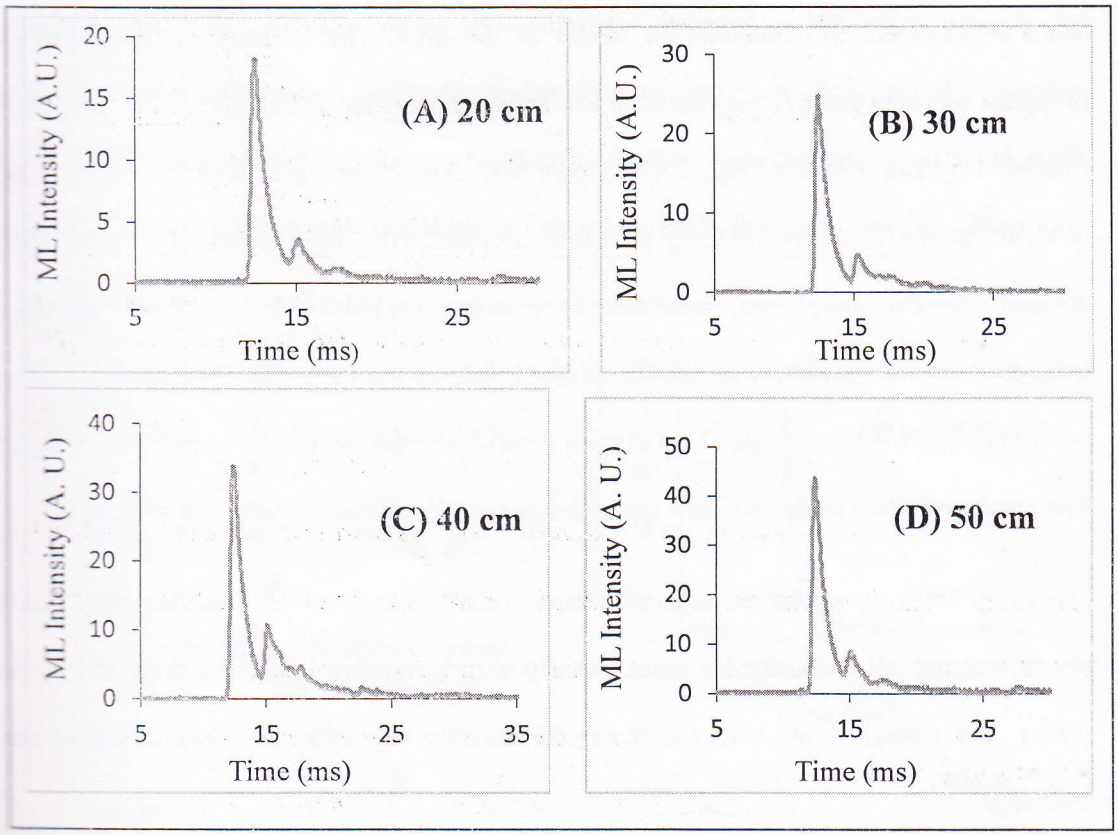

Fig. 25 (a) Change in ML intensity with impact height for 1180Gy of γ- dose.

Mechanoluminescence is associated with a trap- involved process, in which electrons (or holes) dwell in the trap for some time and then recombine with the luminescence center either by traveling in the conduction band (or valence band) or by electron (or holes) tunneling. When the prepared material was fractured, free electrons and holes were generated and the subsequent recombination of electrons with the holes centers gave rise to the light emission. During deformation of $Ca_2Al_2SiO_7$: Ce^{3+} phosphor, a large number of physical processes may occur within very short time intervals, which may excite or stimulate photon emission. ML was measured for different drop heights. The velocity of the moving piston having constant mass

could be changed, by changing the height of the drop. The quantity of $Ca_2Al_2SiO_7$: Ce^{3+} phosphor was kept same (5 mg) for each ML measurement. The $Ca_2Al_2SiO_7$: Ce^{3+} phosphor was irradiated by the γ source. Fig. 25(a) shows ML glow curves measured by applying a load (400gm) to the $Ca_2Al_2SiO_7$: Ce^{3+} phosphor dropped from heights 20, 30, 40 and 50 cm, respectively. The sample was irradiated by γ dose for 1180Gy. It was found that the peak intensity increases linearly with the increasing height of the load. The maximum ML intensity was obtained for 50 cm height. Two distinct peaks are observed in ML intensity vs. time curve. The presence of two peaks indicates some charge transfer process involved in ML process.

Fig. 25(b) shows the characteristics curve of ML intensity vs. impact velocity. The figure shows that the ML intensity increases linearly with increasing impact velocity of the moving piston. As the height of the piston increases the area of newly created surface increases hence the intensity.

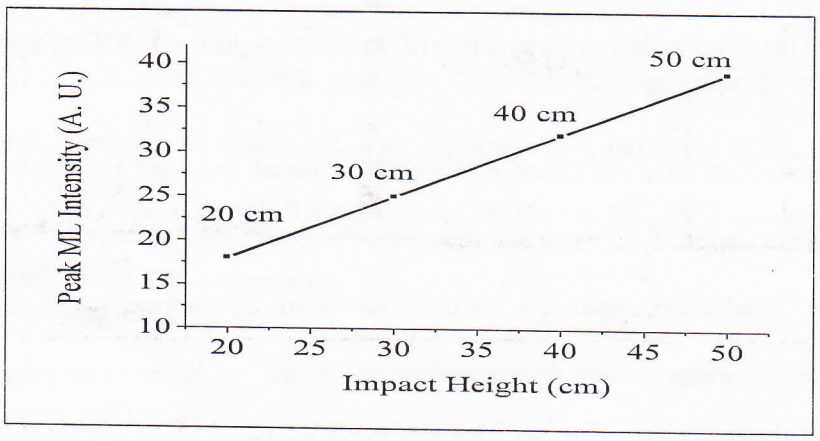

Fig. 25 (b) Peak ML intensity versus Impact height

Fig. 26 shows ML intensity versus time curve for different γ- irradiation time by the impact of same load (400gm). It is clearly visible that the phosphor show the ML intensity linearly increases with increase in γ dose up to 1180Gy. As the γ dose increases, carrier (electron and hole) concentration in trap level increases, which results in the increase in the ML intensity.

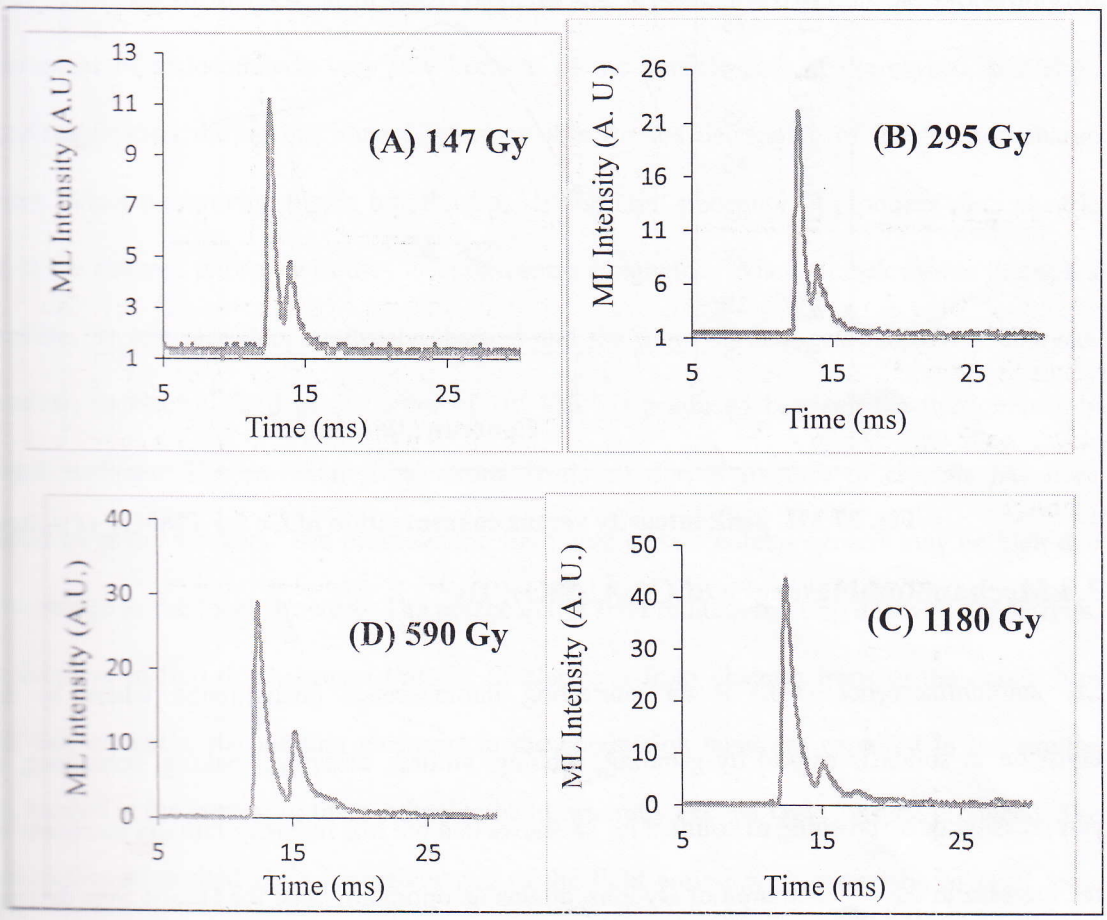

Fig. 26 ML intensity versus time curve for γ- irradiated Phosphor

Fig.27 shows the relationship of ML intensity to the concentration of Ce. The ML emission intensity of the $Ca_2Al_2SiO_7$: Ce^{3+} samples with various concentrations of Ce^{3+} (x = 0.5–4 mol %) under γ - irradiation is shown in the below figure. The ML intensity increases with

increasing concentration of Ce, reaches to the maximum value and then it descends for higher concentration. The highest mechanoluminescence (ML) intensity was obtained for 2mol% of Ce in the $Ca_2Al_2SiO_7$ phosphor.

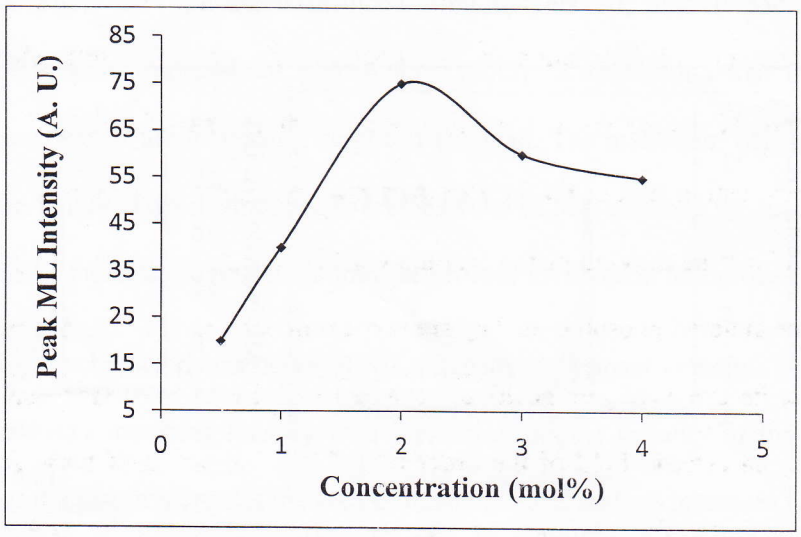

Fig. 27 ML peak intensity versus concentration of Ce for 1180Gy of γ- dose.

3.8 Mechanoluminescence of $Ca_2Al_2SiO_7$: Dy^{3+}

Mechanoluminescence (ML) is an interesting luminescence phenomenon where by light emission in solids is caused by grinding, rubbing, cutting, cleaving, shaking, scratching, and compressing or by crushing of solids. Fig. 28 shows that the ML intensity initially increases with the increase in the concentration of Dy ions, attains an optimum value for 1mol% then decreases with further increase in the concentration of Dy^{3+}. Two peaks have been found in ML Vs Time curve [28 (a)].

It is believed that the fist peak is attributed to the ML produced due to charging of the newly created surface. Since the mechanical energy cannot be supplied directly to the trapped charge carrier, deformation induced intermediate process is responsible for the de-trapping of the

charge carriers. ML is a defect related phenomenon, associated with a trap involved process, in which electrons (or holes) dwell in the trap for some time and then recombine with the luminescence center, either by traveling in the conduction band (or valence band) or by electron (or holes) tunneling. As for ML materials, in particular, there combination process is facilitated by the assistance of dislocation in the crystal. In the present investigation the probability of involvement of dislocation is very low because of the particle size of the crystal, probably, piezoelectrification during the impact is responsible for the detrapping of the trapped charge carriers. When the moving piston hits the $Ca_2Al_2SiO_7:Dy^{3+}$ phosphor, it produces piezoelectric field in the sintered phosphor as they are non-centro symmetric. When a crack moves through a crystallite, its one face gets positively charged and the other surface gets negatively charged. Therefore, an electric field of the order of 10^8 Vm^{-1} is produced between the two oppositely charged surfaces. The emission of electrons produced during fracture of crystals has been reported by many workers. The piezoelectric field near certain defects centers may be high due to the change in the local structure. The piezoelectric field reduces the trap depth of the carriers. The decrease in trap depth causes transfer of electrons from electron traps to the conduction band. Subsequently, the moving electrons in the conduction band are captured in the excited state, located at the bottom of the conduction band, whereby excited Dy^{3+} ions are produced. The de-excitation of excited Dy^{3+} ions gives rise to the light emission characteristic of Dy^{3+} ions, which can be attributed to $^4F_{9/2} \rightarrow {}^6H_{15/2}$, $^4F_{9/2} \rightarrow {}^6H_{13/2}$ and $^4F_{9/2} \rightarrow {}^6H_{11/2}$ respectively of Dy^{3+} ions.

The occurrence of second peak, which occurs in the post deformation region, may be due to the captures of carriers by the shallow traps lying away from the newly created surfaces where the electric field near the surface is not so effective. The release of trapped charge carriers from

shallow traps may take place later on due to thermal vibration of lattices and therefore a delayed ML (second peak) may be produced, which may lie in the post deformation region of the phosphor.

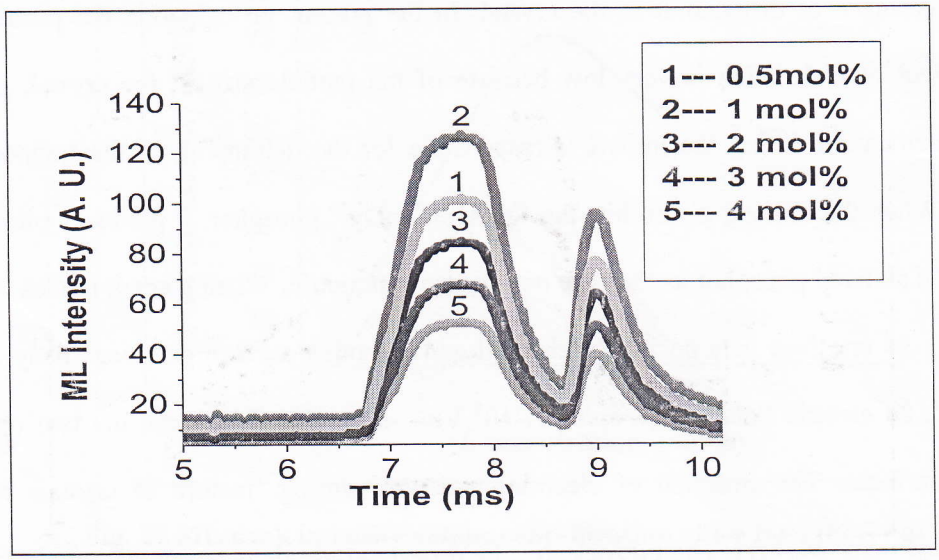

Fig. 28 (a) ML intensity verses time curve for different Dy^{3+} concentration

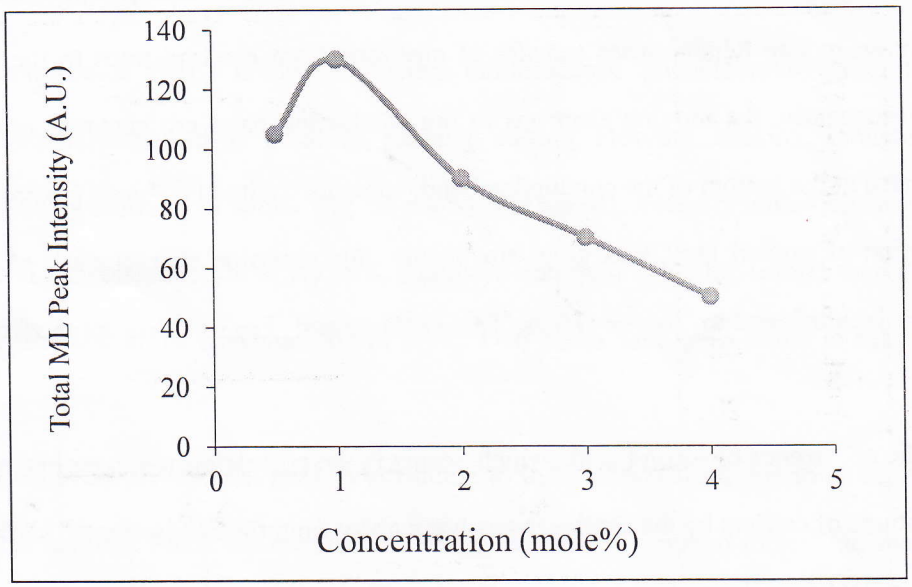

Fig. 28 (b) Variation of peakML intensity by Dy^{3+} concentration variation

Fig. 29 shows the gamma dose dependence of ML intensity. It was observed that ML intensity increases with the increase in gamma dose because more charge carriers are trapped with the increase in gamma dose, after that it seems to be saturated as no more traps are available for trapping.

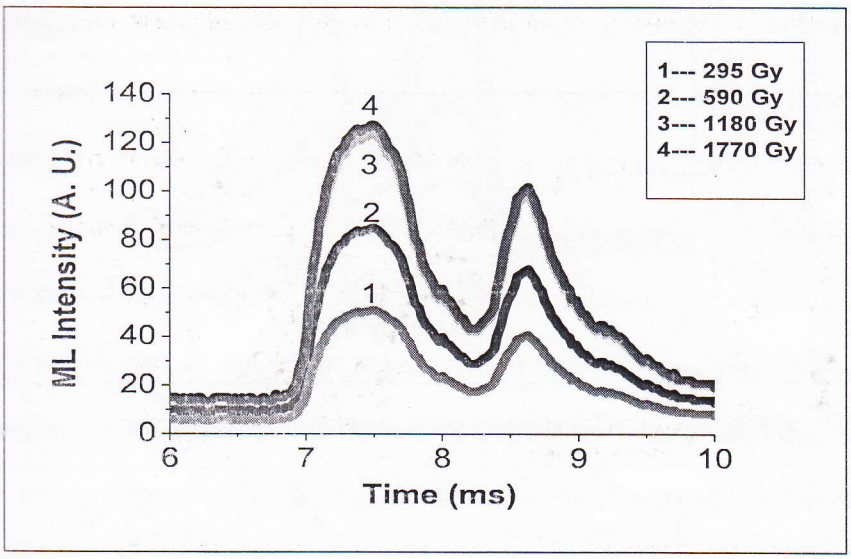

Fig. 29(a) ML intensity versus time curve for γ- irradiated phosphor

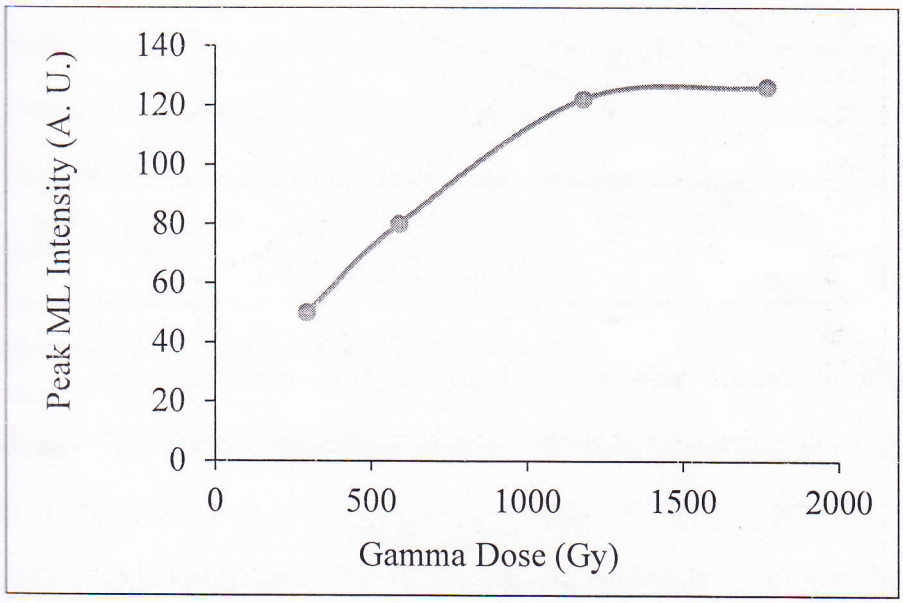

Fig. 29 (b) Dependence of Peak ML intensity on γ– dose

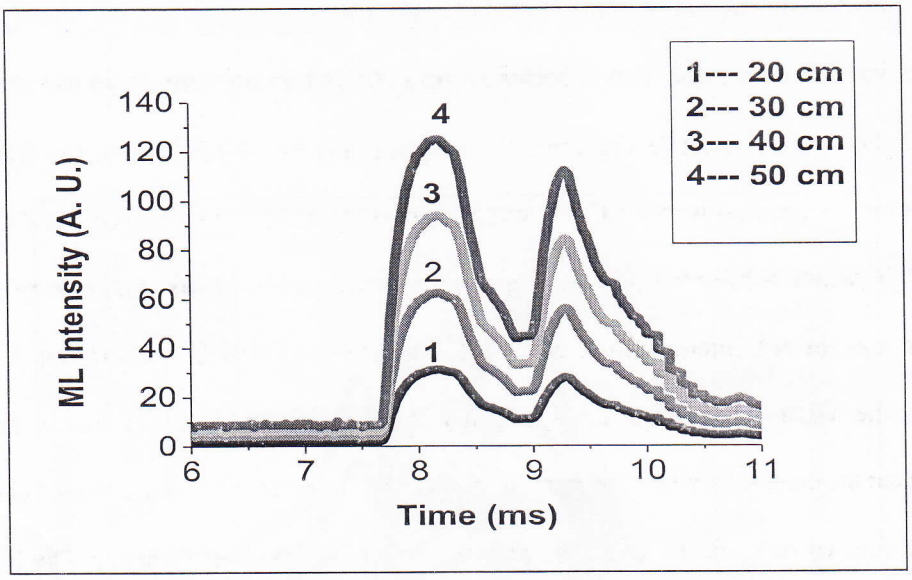

Fig. 30 (a) Change in ML intensity with impact height for 1180 Gy of γ-dose

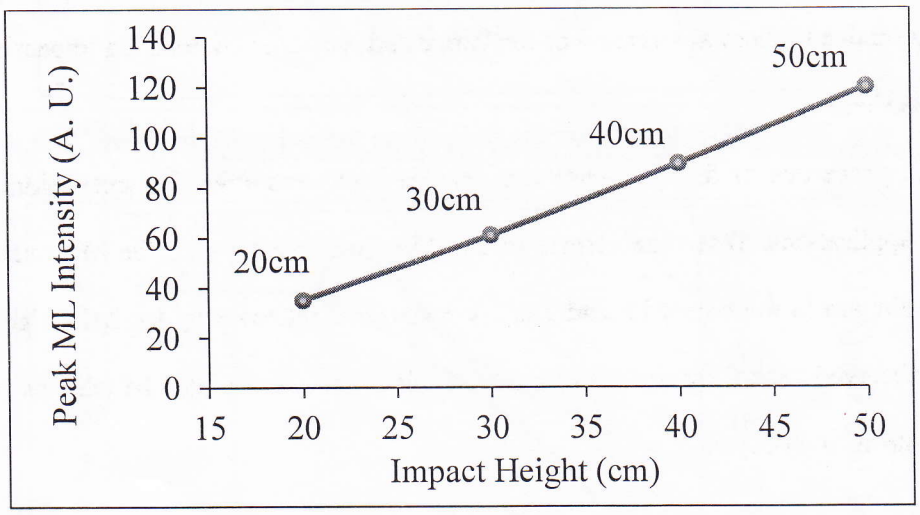

Fig. 30 (b) Peak ML intensity versus Impact height for 1180 Gy of γ- dose

Fig.30 (a) shows the characteristics curve between ML intensity versus time for $Ca_2Al_2SiO_7:Dy^{3+}$ phosphor at different heights. The experiment was carried out for a fixed moving piston (400 gm) dropped with different heights 20, 30, 40, 50 cm. It is evident that the ML intensity increases with the increase of falling height of moving piston, showing the ML peak intensity

maximum at 50 cm height. Because the experimental limitation the maximum height from which the piston is dropped is 50 cm.

Fig.30 (b) shows the curve between peak ML intensity versus impact velocity of $Ca_2Al_2SiO_7:Dy^{3+}$ phosphor. The ML intensity increases linearly with increasing the falling height of the moving piston; that is, the ML intensity depends upon the impact velocity of the moving piston [$\sqrt{2gh}$ (where = h, is the different heights of moving piston)]. As the velocity of moving piston increases the ML intensity increases due to creation of new surface on impact.

For the ML Figures (Figures 28, 29, 30), the first ML peak occurs due to charging of newly created surface. And when the moving piston hits the phosphor then effect of piston is not uniform on the whole surface area of the phosphor as it is in powder form. So The ML peak is broad. While the second peak is due to release of carriers from the shallow traps which takes place later on due to thermal vibration of the lattice and it does not depend on impact on surface area so it is sharp.

ML properties of this phosphor can provide high sensitivity for smart skin and self-diagnosis applications. When the surface of an object was coated with the ML materials, the stress distribution in the object beneath the layer could be reflected by the ML brightness and could be observed. Based on the above analysis this phosphor can also be used as sensors to detect the stress of an object.

3.9 Mechanoluminescence of $Ca_2Al_2SiO_7: Eu^{3+}$

Mechanoluminescence (ML) is an interesting luminescence phenomenon where by light emission in solids is caused by grinding, rubbing, cutting, cleaving, shaking, scratching, and compressing or by crushing of solids. Fig. 31 shows that the ML intensity initially increases with

the increase in the concentration of Eu ions, attains an optimum value for 2mol% then decreases with further increase in the concentration of Eu^{3+}. Two peaks have been found in ML Vs Time curve [31(a)]. Since the mechanical energy cannot be supplied directly to the trapped charge carrier, deformation induced intermediate process is responsible for the de-trapping of the charge carriers. ML is a defect related phenomenon, associated with a trap involved process, in which electrons (or holes) dwell in the trap for some time and then recombine with the luminescence center, either by traveling in the conduction band (or valence band) or by electron (or holes) tunneling. As for ML materials, in particular, there combination process is facilitated by the assistance of dislocation in the cryst. In the present investigation the probability of involvement of dislocation is very low because of the particle size of the crystal; probably, piezoelectrification during the impact is responsible for the detrapping of the trapped charge carriers. The occurrence of second peak, which occurs in the post deformation region, may be due to the captures of carriers by the shallow traps lying away from the newly created surfaces where the electric field near the surface is not so effective. The release of trapped charge carriers from shallow traps may take place later on due to thermal vibration of lattices and therefore a delayed ML (second peak) may be produced, which may lie in the post deformation region of the phosphor.

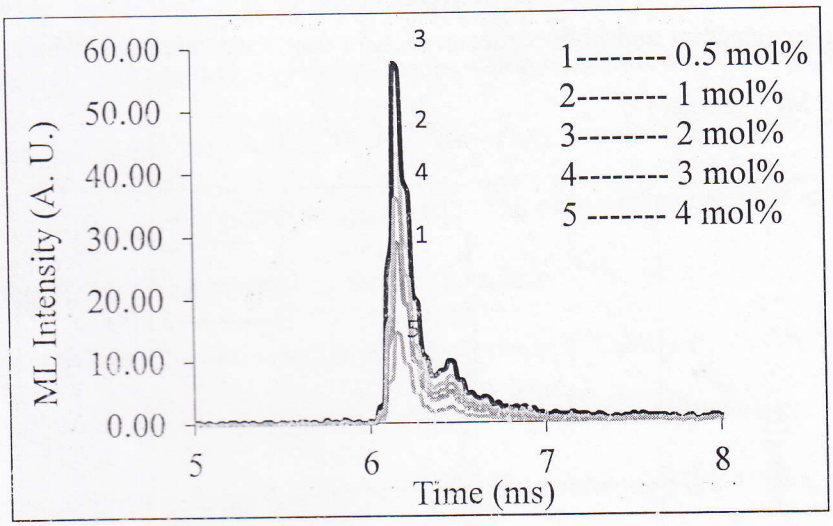

Fig. 31 (a) ML intensity verses time curve for different Eu^{3+} concentration for γ dose of 1770 Gy

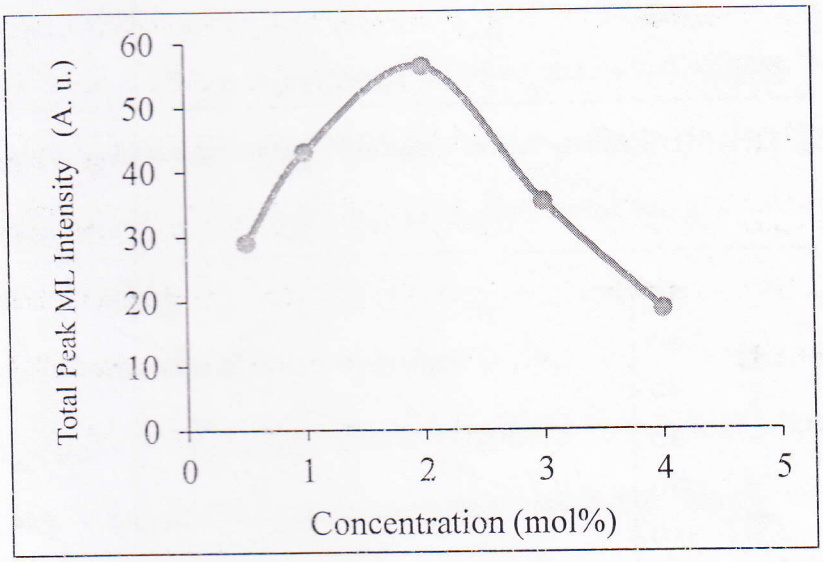

Fig. 31 (b) Variation of peak ML intensity by Eu^{3+} concentration variation

Fig. 32 shows ML intensity versus time curve for different γ- irradiation time by the impact of same load (400gm), dropped with same height 50 cm. It is clearly visible that the phosphor show the ML intensity linearly increases with increase in γ dose up to 1770Gy. As the γ dose

increases, carrier (electron and hole) concentration in trap level increases, which results in the increase in the ML intensity.

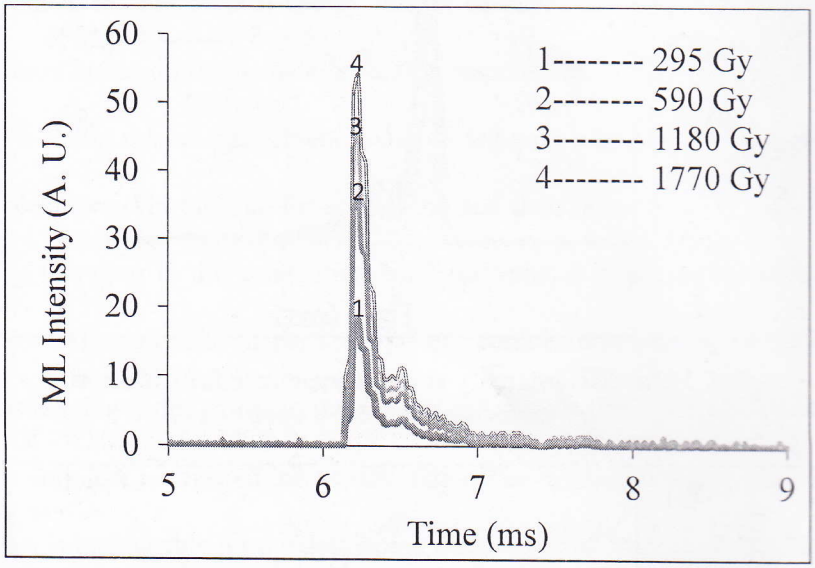

Fig. 32(a) ML intensity versus time curve for γ- irradiated phosphor

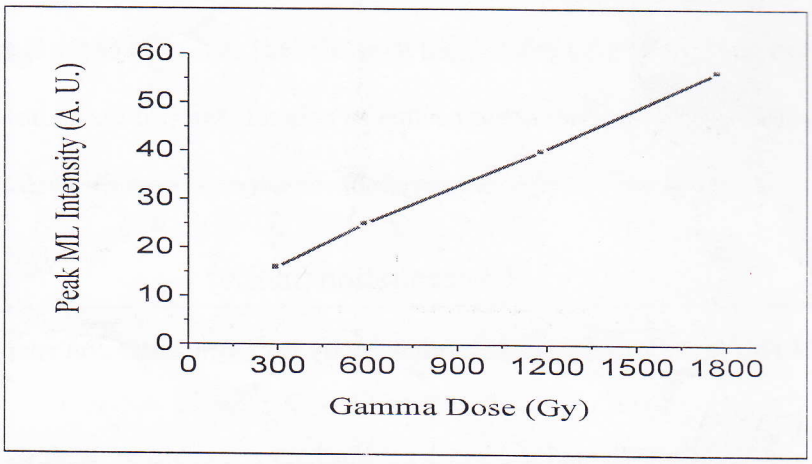

Fig. 32 (b) Dependence of Peak ML intensity on γ– dose

Fig.33 (a) shows the characteristics curve between ML intensity versus time for $Ca_2Al_2SiO_7:Eu^{3+}$ (2mol %) phosphor at different heights. The experiment was carried out for a fixed moving

lling height of the moving piston; that is, the ML intensity depends upon the impact velocity of ne moving piston [√2gh (where = h, is the different heights of moving piston)]. As the velocity f moving piston increases the ML intensity increases due to creation of new surface on impact. Vhen the moving piston hits the $Ca_2Al_2SiO_7:Eu^{3+}$ phosphor, it produces piezoelectric field in the intered phosphor as they are non-centro symmetric. The piezoelectric field near certain defects enters may be high due to the change in the local structure. The piezoelectric field reduces the rap depth of the carriers. The decrease in trap depth causes transfer of electrons from electron raps to the conduction band. Subsequently, the moving electrons in the conduction band are captured in the excited state, located at the bottom of the conduction band, whereby excited ions are produced. The subsequent recombination of electrons with the hole centers gives rise to the light emission. ML properties of this phosphor can provide high sensitivity for smart skin and self-diagnosis applications. When the surface of an object was coated with the ML materials, the stress distribution in the object beneath the layer could be reflected by the ML brightness and could be observed. Based on the above analysis this phosphor can also be used as sensors to detect the stress of an object.

Conclusions and Significance of the present work:

The work done in the present project was carried out as planned originally. Some rare-earth doped Calcium Alumino silicate phosphors were prepared by Combustion Synthesis which appears to be a more feasible method for production. The identification of the phosphors was done by XRD, TEM, SEM, EDX studies. The phase structure of the rare earth doped $Ca_2Al_2SiO_7$ phosphor is consistent with standard tetragonal crystallography. TEM results also confirms nano size of the prepared phosphors.

This present work is aimed at searching for the white light emitting long-lasting phosphors. Under the ultra-violet excitation, the prepared $Ca_2Al_2SiO_7:Dy^{3+}$phosphor would emit blue, yellow and red light with peak at 484 nm, 583 nm and 680 nm corresponds. The red light emission peaking at 680 nm is weak compared to the blue emission (484 nm) and yellow emission (583 nm). The PL emission exhibited a white light which was confirmed from the calculated CIE coordinates which were found to be very close to standard white light for human eyes.

Dy^{3+} ions have potential application for fluorescent tubes, colour televisions and glass lasers and long lasting mercury free fluorescence lamp and white light-emitting diodes (LEDs). In these devices, luminescent materials absorb energy generated from cathode ray or ultraviolet (UV) radiation and then convert it to visible light. Dy^{3+} ion is also a good activator for preparation of electron trapping luminescence materials. Dy^{3+}activated luminescent materials are single phase white phosphors and high luminous white light emission resulted from a single phase phosphor is expected.

$Ca_2Al_2SiO_7:Ce^{3+}$ has been prepared and their Mechanoluminescence, Thermoluminescence and photoluminescence properties are studied. This phosphor is regarded as a new generation of long afterglow materials because the melilites are more stable than the aluminates.

We have investigated the Photoluminescence, Mechanoluminescence and Thermoluminescence phenomena in the $Ca_2Al_2SiO_7:Eu^{3+}$ phosphor. The excitation spectra indicate that the phosphor can be effectively excited by near ultraviolet (NUV) light, making it attractive as conversion phosphor for LED applications. The $Ca_2Al_2SiO_7:Eu^{3+}$ phosphor exhibits bright orange - red emission excited by 394 nm. CIE chromaticity diagram confirms

$Ca_2Al_2SiO_7:Eu^{3+}$ phosphor exhibits efficient orange - red emission and excellent color stability, indicating that it has favorable properties for application as near ultraviolet LED conversion phosphor. The gamma irradiated ML and TL study shows that the intensity depends upon the gamma dose given to the system, it shows linear response with gamma irradiation which suggests the possible application in ML and TL dosimetry.

Acknowledgement

The authors express their sincere thanks to CCOST, Raipur for providing financial assistance through the Research Project **No. 15031/CCOST/MRP/ 2013: 29/03/2014**. We are thankful to Prof. S. K. Pandey (Vice- Chancellor, Pt. Ravishankar Shukla University, Raipur), Prof. R. C. Agrawal (Ex - Head, SoS in Physics and Astrophysics, Pt. R. S. U. Raipur), Prof. R. N. Baghel (Ex - Head of Department, SoS in Physics and Astrophysics, Pt. R. S. U. Raipur) for constant encouragement and support. We are also thankful to all my friends, colleagues and co-workers who helped me directly/ indirectly in completing the project. We wish to thanks my students Ms. Geetanjali Tiwari, who worked day & night untiringly and obediently.

References:

[1] P. Niel. Yocom, J. Soc. Inform. Display, (1996), 4, 149-152.

[2] D. E. Harrison and V. Hoffman, J. Electrochemical. Soc., (1959), 106, 800-804.

[3] T. Aitasalo, J. Holsa, M. Lastusaari, J. Legendziewicz, J. Niittykoski and F. Pelle, Opt. Mater., (2004), 26, 107-112.

[4] G. Tiwari, N. Brahme, R. Sharma, D.P. Bisen, S. K. Sao and U. K. Kurrey, J. of Mater. Sci: Mater. in Electron., (2016), 27, 6399–6407.

[5] N. Kodama, N. Sasaki, M. Yamaga and Y. Masui, J. Lumin., (2001), 19, 94–95.

[6] N. Kodama, Y. Tanii and M. Yamaga, J. Lumin., (2000), 1076, 87–89

[7] X.J. Wang, D.D. Jia and W.M. Yen, J. Lumin., (2003), 34, 102–103.

[8] Z. L. Wang, H.B. Liang, L.Y. Zhou, H. Wu, M.L. Gong and Q. Su, Chem. Phys. Lett., (2005), 412, 313-316.

[9] X.M. Zhang, L.F. Liang, J.H. Zhang and Q. Su, Mater. Lett., (2005), 59, 749-753.

[10] J.K. Park, C.H. Kim, S.H. Park, H.D. Park and S.Y. Choi, Appl. Phys. Lett., (2004), 84, 1647-1649.

[11] S. Dalmasso, B. Damilano, C. Pernot, A. Dussaigne, D. Byrne, N. Grandjean, M. Leroux and J. Massies, . Physica status solidi (a)., (2002), 192,139–143.

[12] C.H. Kuo, J.K. Sheu, S.J. Chang, Y.K. Su, L.W.Wu, J.M. Tsai, C.H. Liu and R.K. Wu, Japan. J. Appl. Phys., (2003), 42, 2284-2287.

[13] S. Neeraj, N. Kijima and A.K. Cheetham, Chem. Phys. Lett., (2004), 387, 2-4.

[14] X. J. Wang, D. Jia and W. M. Yen, J. Lumin., (2003), 102, 34-37.

[15] Q. Zhang, J. Wang, M. Zhang and Q. Su, Appl. Phys. B: Lasers Opt., (2008), 92, 195 - 198.

[16] G. Tiwari, N. Brahme, R. Sharma, D. P. Bisen, S. K. Sao and M. Singh, J. Bio. And Chemi. Lumi., (2015), 31, 793–801.

[17] R. Chen, J. Appl. Phys., (1969), 40, 570 –585.

[18] M. Akiyama, N. X. Chao, H. Matsui, K. Nonaka and T. Watanabe, Appl. Phys. Lett., (1999), 75, 2548-2550.

[19] L. M. Sweeting, Chem. Mater., (2001), 13, 854–870.

[20] G. Tiwari, N. Brahme, R. Sharma, D. P. Bisen, S. K. Sao and S. J. Dhoble, RSC Advan., (2016), 6, 49317-49327.

[21] Y. Jia, Y. Ming, and J. Weiyi, Opt. Mater., (2006), 28, 974–979.

Date:

Signature of PI

Nameeta 14/09/2016

Dr. Mrs. Nameeta Brahme

Dr. Nameeta Brahme
Principal Investigator
Research Project C COST
S.O.S. in Physics & Astrophysics
Pt. R. S. University, RAIPUR

Signature of Co-PI

DPBisen 14/09/2016

Dr. D.P. Bisen

Dr. D.P. Bisen
Professor
SOS in Physics & Astrophysics
Pt. R.S. University, Raipur (C.G.)

Nameeta 14/09/2016

Forwarded by

(Dr. Nameeta Brahme)
Professor & Head
S.O.S. in Physics & Astrophysics
Pt. Ravishankar Shukla University
Raipur 492010